ISSN 1063-7729, Astronomy Reports, 2022, Vol. 66, No. 8, pp. 669–692. © Pleiades Publishing, Ltd., 2022.
Russian Text © The Author(s), 2022, published in Astronomicheskii Zhurnal, 2022, Vol. 99, No. 8, pp. 650–674.

Comparison of the Angles between the Magnetic Moment and Rotation Axis for Two Groups of Radio Pulsars

Z. V. Ken'ko[a] and I. F. Malov[b, *]

[a] *Pushchino State Natural Science Institute, Pushchino, Russia*

[b] *Lebedev Physical Institute, Russian Academy of Sciences, Pushchino Radio Astronomy Observatory, Astrospace Center, Pushchino, Russia*

**e-mail: malov@prao.ru*

Received April 11, 2022; revised May 28, 2022; accepted June 21, 2022

Abstract—Angles β between the rotation axis and the magnetic moment are calculated in two groups of radio pulsars with different periods ($P > 2$ s and 0.1 s $< P <$ 2 s). Two methods have been used. The first method is based on the observed pulse widths and provides the minimum values of angle β_1. The distributions of these angles differ significantly for these groups of objects. The second method uses polarization data to calculate more accurate values β_2. There is a trend for bimodality in the distribution of β_2 values for pulsars with $P > 2$ s. The closeness of the mean β_2 values (47.6° for long-period pulsars and 35.6° for sources with shorter periods) does not allow us to explain the previously discovered difference in the behavior of these two groups in the (dP/dt)–(P) diagram by a decrease in the role of magnetic dipole radiation due to a decrease in β. Our analysis showed that the observed difference can be explained by the different dependence of the pulsar wind and magnetic dipole braking on the period of the pulsar. The deceleration of pulsars with $P > 2$ s is mainly caused by the pulsar wind.

Keywords: neutron stars, radio pulsars, structure of the magnetosphere, deceleration mechanisms

DOI: 10.1134/S1063772922090050

1. INTRODUCTION

One of the tools for analyzing the evolutionary paths of radio pulsars is still the study of the position of these objects in the (dP/dt)–(P) diagram, which describes the dependence of the derivative of the period between successive pulses on the period itself. This is due to the fact that these values are measured directly during sufficiently long observations and are not related to various assumptions about the nature of pulsars and their models. In [1], the corresponding diagrams were studied for three groups of pulsars with different period values: $P > 2$ s, 0.1 s $< P <$ 2 s, and $P <$ 0.1 s. It was shown that the rotation of pulsars in the first group is slowed down by the removal of the angular momentum by relativistic particles (pulsar wind). In this case, the loss of rotational energy is described by the following expression [2]:

$$I\Omega\frac{d\Omega}{dt} = -\frac{L_p^{1/2}BR_*^3\Omega^2}{(6c^3)^{1/2}}. \quad (1)$$

Here, I is the moment of inertia of the neutron star, R_* is its radius, $\Omega = 2\pi/P$ is the angular velocity of rotation, B is the magnetic field on the surface, L_p is the wind power, and c is the speed of light.

In the second group, the pulsar wind is joined by the magnetic dipole radiation of the neutron star [3]:

$$I\Omega\frac{d\Omega}{dt} = -\frac{B^2R_*^6\Omega^4\sin^2\beta}{6c^3}. \quad (2)$$

The sources of the third group are decelerated by both mechanisms. It was suggested [1] that the contribution of the magnetic dipole radiation depends on the value of angle β between the magnetic moment of a neutron star and its rotation axis. Indeed, it follows from expression (2) that the smaller this angle with other parameters being equal, the smaller the contribution of the magnetic dipole mechanism. To verify this assumption, it is necessary to calculate angle β for pulsars with different periods and analyze the difference in this angle in different populations.

During all the years of pulsar studies, numerous attempts were made to calculate the β angles using various methods [4–8]. It was also important to understand how this angle evolves with the age of the pulsar. In [9], a model of the magnetosphere was constructed, in which angle β should increase with time, i.e., pulsars tend to become orthogonal rotators. However, further magnetohydrodynamic calculations [10] showed that the inclination of the magnetic moment

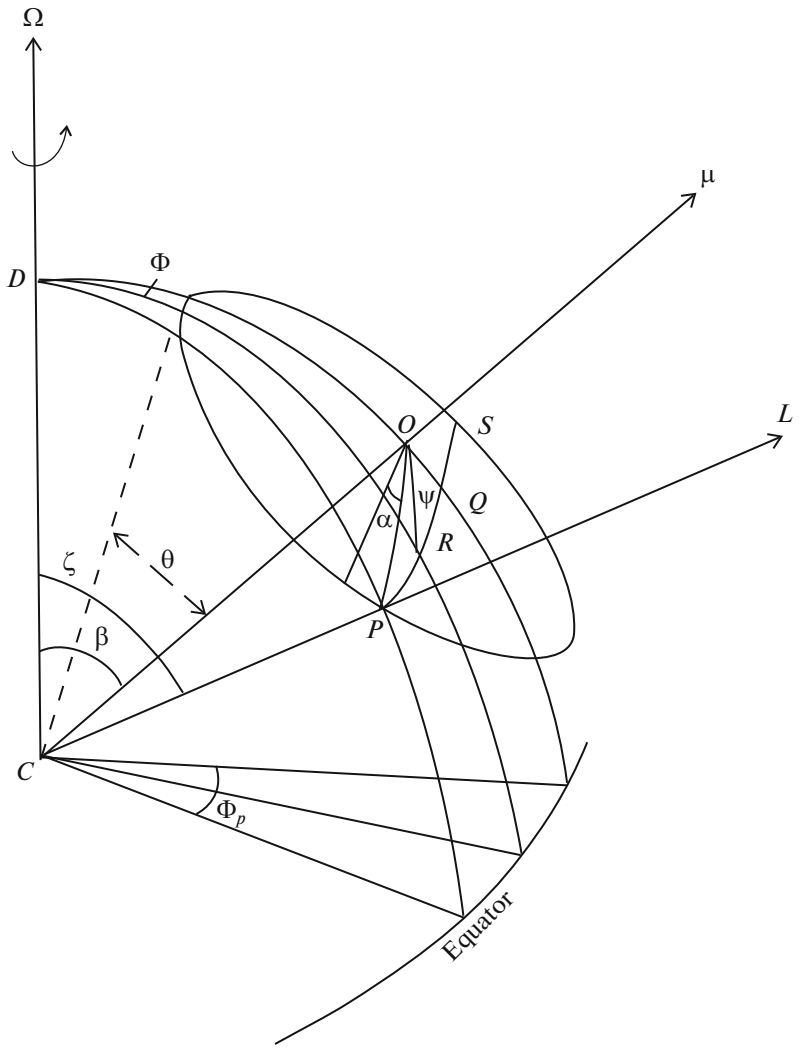

Fig. 1. Geometry of a pulsar radiation cone in the polar cap model: Φ_p is the observed pulse halfwidth, $\vec{\Omega}$ is the rotation axis of the pulsar, μ is the vector of the dipole magnetic moment, L is the observer's line of sight, θ is the angular radius of the radiation cone, ζ is the angle between the line of sight and the rotation axis, β is the angle between the rotation axis and the magnetic moment vector, ψ is the position angle of the radiation polarization plane, and Φ is the longitude.

to the axis of rotation decreases with age following a power law.

We analyze the difference in angle β for two groups of pulsars with $P > 2$ s and $0.1\,\text{s} < P < 2$ s. As for objects with $P < 0.1$ s, relativistic effects begin to play a role in them [11] and the calculation of β may require other methods, which differ from those described in the next section.

2. METHODS USED TO CALCULATE ANGLE β

Further, we use the polar cap model shown in Fig. 1. Spherical trigonometry allows writing an equation that relates angles β, ζ, and θ:

$$\cos\theta = \cos\beta\cos\zeta + \sin\beta\sin\zeta\cos\Phi. \quad (3)$$

Two more equations are needed to determine all three angles.

The simplest estimation method is associated with the assumption that the line of sight passes through the center of the radiation cone. In this case,

$$\beta = \zeta, \quad (4)$$

and the statistical dependence of the pulse width at the 10% level on the period $W_{10}(P)$ can be used as the third equation, assuming that the observed profile width is related to the position of the radiation cone relative to the rotation axis. The real radius of the cone will correspond to $\beta = 90°$, which in the (W_{10})–(P) diagram is determined by the lower boundary of the array of the observed values:

$$\theta = W_{10\,\min}(P)/2. \quad (5)$$

This makes it possible to estimate angle β based on Eq. (3) using the following expression:

$$\beta = \arcsin\left(\frac{\sin\frac{W_{10\,\min}}{4}}{\sin\frac{W_{10}}{4}}\right). \quad (6)$$

Since we assumed that the observed pulse broadening is associated solely with the approach of the radiation cone to the rotation axis of the pulsar, the values of the β angle calculated by formula (6) represent the lower limits of this angle.

In what follows, we will use the pulsar parameters given in the ATNF catalog (latest version 1.67) [12].

It is generally accepted that the observed radio emission from pulsars is generated by the curvature radiation mechanism. In this case, the position angle ψ of linear polarization is determined by the projection of the magnetic field, and its dependence on other angles can be represented as [13]

$$\tan\psi = \frac{\sin\beta\sin\Phi}{\sin\zeta\cos\beta - \cos\zeta\sin\beta\cos\Phi}. \quad (7)$$

The observational data show that the variation of the position angle for many pulsars is measured only within the main pulse in a small interval of longitudes Φ. The rate of variation of the position angle reaches its maximum $(d\psi/d\Phi)_{\max}$ when the line of sight crosses the meridian at which the magnetic axis is located (Φ = 0)

$$\left|\frac{d\psi}{d\Phi}\right|_{\max} = \frac{\sin\beta}{\sin(\zeta-\beta)}. \quad (8)$$

The Φ_p value for the observed profile is determined by Eq. (3) and is given by the angle β (apparent pulse broadening when approaching the axis of rotation) and the angular distance (ζ – β) at which the line of sight intersects the radiation cone. The latter effect reduces the observable width Φ_p. The contribution of each of these effects is not known in advance; therefore, on average, they can be considered equal, i.e., compensating each other. The θ(*P*) dependence can then be determined by a straight line inscribed in the $W_{10}(P)$ array using the least squares method, and we can set

$$\theta = \frac{\langle W_{10}\rangle}{2}. \quad (9)$$

Expressions (3), (8), and (9) form a system of three equations, which is reduced through transformations to an algebraic equation of the 4th degree:

$$\begin{aligned} &C(1-D)^2y^4 + 2C(1-D)y^3 \\ &+ [1 + 2C^2D(1-D)]y^2 + 2C(D-B^2)y \\ &+ C^2D^2 - B^2(1+C^2) = 0, \end{aligned} \quad (10)$$

where the following notations are introduced:

$$\begin{aligned} &B = \cos\theta, \quad C = |d\psi/d\Phi|_{\max}, \\ &D = \cos\langle W_{10}\rangle/2, \quad y = \cos\zeta. \end{aligned} \quad (11)$$

Using expressions (11), relation (8) can be rewritten as

$$\tan\beta = \frac{C(1-y^2)^{1/2}}{1+Cy}. \quad (12)$$

Solving Eq. (10) with respect to *y*, we find the required angle β using (12).

Equation (10) has 4 solutions, from which 4 β values are found. Some solutions may be complex and should be discarded. The sign of the derivative $C = (d\psi/d\Phi)_{\max}$ cannot be determined from the main pulse observations only, since the $d\Phi$ sign is not known, and the pulsar can rotate both clockwise and counterclockwise; therefore, it is necessary to solve the system of equations (10) and (12) at $C > 0$ and $C < 0$. Equation (10) can give a negative value $y = \cos\zeta$. This corresponds to $\zeta > 90°$, which is quite possible in real pulsars.

In the calculation of angles β by this method, we used the catalog of polarimetric data for 600 pulsars [14]. Objects in globular clusters and binary systems, where their parameters are affected by companions, were excluded. The following factors were also taken into account:

(1) The jump of the position angle by 180° corresponds to its simple continuation, i.e., the polarimetric curves should be "sewn" at the discontinuity point. An example of this case is shown in Fig. 2.

(2) Jumps by 90° or smaller values indicate the presence of another mode (or other polarization modes), and such pulsars were excluded from further consideration.

(3) Sources with a stretched right "tail" in their pulses were also excluded. These "tails" are caused by scattering in the medium between the pulsar and the observer, which can significantly distort the polarization properties.

(4) On S-shaped ψ(Φ) dependences, the maximum derivative corresponds to the rectilinear part of the curve.

It should be noted that the solution of the system of equations (10) and (12) exists not for any values *B*, *C*, and *D* obtained from observations. This may mean that the considered model of the behavior of the position angle does not work in certain pulsars.

Angle β can be also determined using other methods [11], but we will restrict ourselves to those considered in this section.

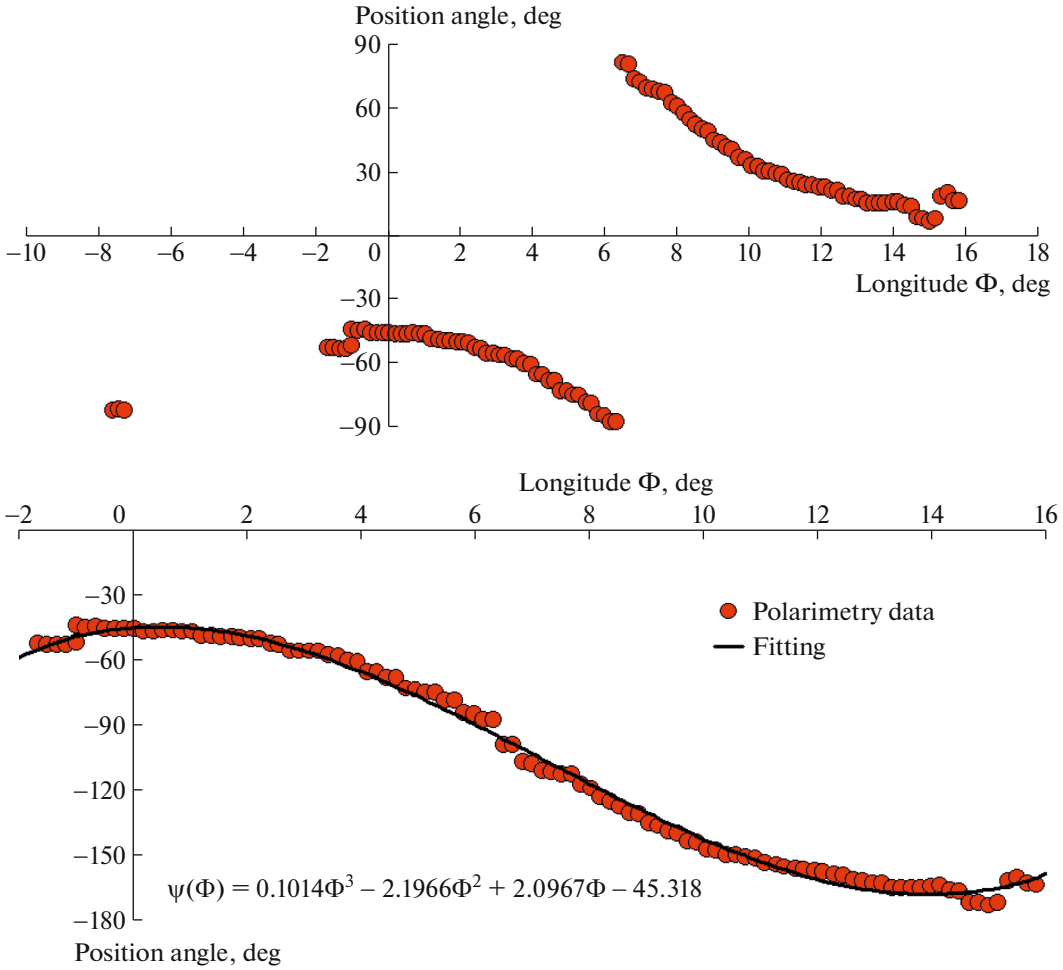

Fig. 2. Top: digitized profile of the position angle ψ(Φ) within the pulse of the pulsar J2346–0609 according to the catalog data [14]; bottom: "sewn" branches of ψ(Φ) and their fitting with a polynomial function: $\psi(\Phi) = 0.1014\Phi^3 - 2.1966\Phi^2 + 2.0967\Phi - 45.318$.

3. RESULTS OF THE CALCULATIONS OF ANGLE β

As already mentioned, we use the data from the catalogs [12, 14] for the analysis.

For further calculations, we need to express the pulse width W in degrees:

$$W_{10}\ [^\circ] = 360^\circ \frac{W_{10}\ [\mathrm{ms}]}{P\ [\mathrm{ms}]}. \quad (13)$$

Figure 3 shows the (W_{10})–(P) diagram for pulsars with $P > 2$ s.

For the range $0.1 < P < 2$ s, the resulting sample contained 1381 pulsars with known W_{10} values; in the range $P > 2$ s, the sample included 119 pulsars (see Tables 1, 2).

For the sample with $P > 2$ s,

$$\log(W_{10\,\mathrm{min}}\ [^\circ]) = -0.582 \log(P\ [\mathrm{s}]) + 0.930, \quad (14)$$

or

$$W_{10\,\mathrm{min}}\ [^\circ]) = 8.5^\circ P^{-0.58}. \quad (15)$$

It should be emphasized that the $W_{10}(P)$ dependences can differ significantly between samples of pulsars, so we separately plotted the diagram similar to Fig. 3 for the sources with $0.1 < P < 2$ s (Fig. 4). The lower boundary for the sample with $0.1 < P < 2$ s is described by the equation

$$\log(W_{10\,\mathrm{min}}\ [^\circ]) = -0.062 \log(P\ [\mathrm{s}]) + 0.555, \quad (16)$$

hence

$$W_{10\,\mathrm{min}}\ [^\circ]) = 3.6^\circ P^{-0.06}. \quad (17)$$

Using expressions (14) and (17) and the catalog W_{10} values, we calculated angles β_1 for the two groups of pulsars under study (see Table 1).

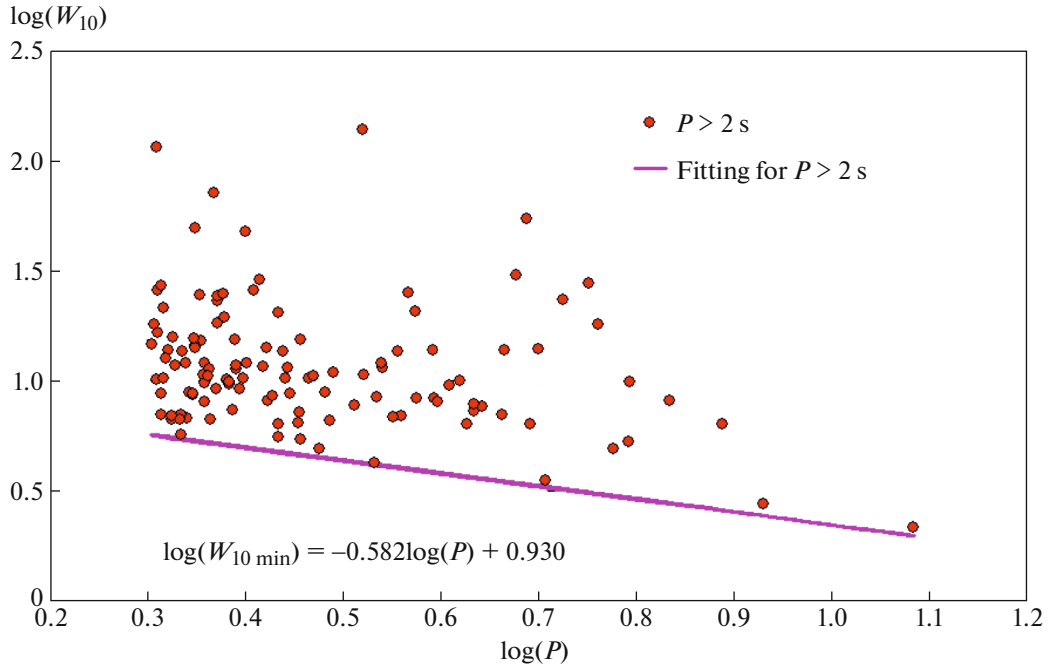

Fig. 3. Pulse width as a function of the period for radio pulsars with $P > 2$ s.

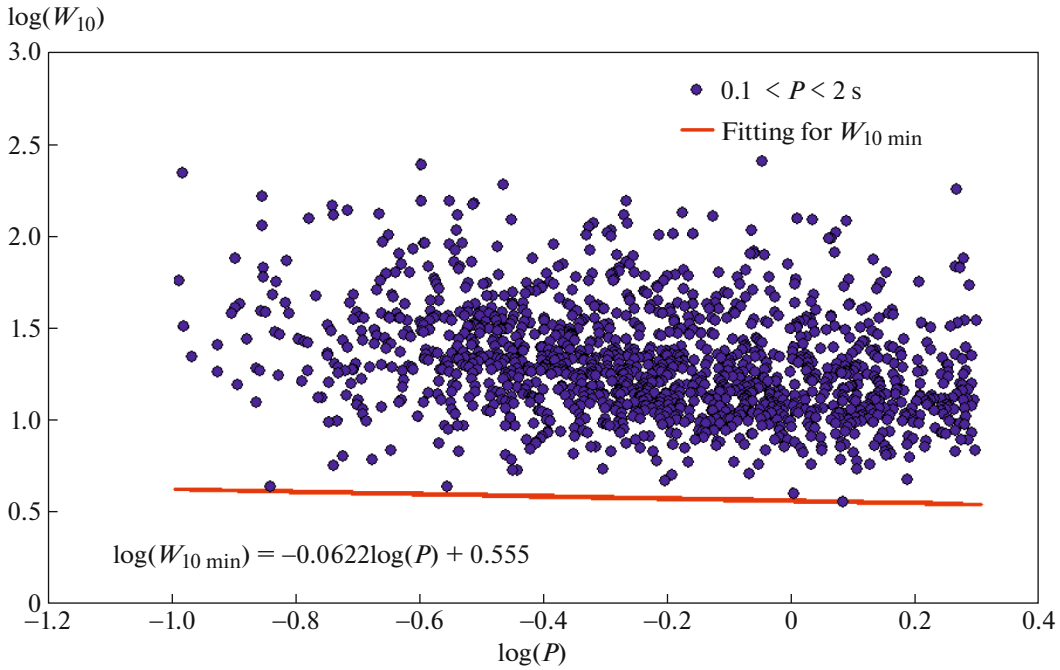

Fig. 4. Pulse width as a function of the period for the sample with $0.1 < P < 2$ s.

Figure 5 shows the β_1 distribution histograms for two samples of pulsars normalized to the total number N of pulsars in the sample.

To compare the statistical difference between the two distributions, the Kolmogorov–Smirnov test was used. The maximum difference $d_{\max}$ between the counts in two histograms was 0.285 (the counts were normalized to the number N of pulsars in the samples). The Kolmogorov quantile was calculated using the formula

$$\lambda = d_{\max}\sqrt{\frac{N_1 N_2}{N_1 + N_2}}, \qquad (18)$$

Table 1. Angle β values for the sample of pulsars with periods $0.1 < P < 2$ s

No.	Name	β_1, deg	β_2, deg	No.	Name	β_1, deg	β_2, deg	No.	Name	β_1, deg	β_2, deg
1	J0006+1834	2.1	—	46	J0242+62	9	—	91	J0533+0402	23.6	—
2	J0014+4746	4.9	—	47	J0243+6027	10.1	—	92	J0536–7543	7.4	39.9
3	J0025–19	7.8	—	48	J0255–5304	28	—	93	J0540+3207	18.7	—
4	J0026+6320	4.1	—	49	J0301+35	7.9	—	94	J0540–7125	10.4	61.2
5	J0033+57	10.2	—	50	J0302+2252	11.6	—	95	J0555+3948	12.4	—
6	J0033+61	20.6	—	51	J0304+1932	12.8	77.5	96	J0601–0527	10	—
7	J0034–0721	4.5	—	52	J0324+5239	2.6	—	97	J0608+00	20.2	—
8	J0038–2501	10.7	—	53	J0325+6744	29.6	—	98	J0611+1436	5.1	—
9	J0040+5716	27	—	54	J0329+1654	14	—	99	J0612+3721	10.4	—
10	J0048+3412	22.4	—	55	J0332+5434	13.4	—	100	J0612+37216	10.3	—
11	J0051+0423	6.4	—	56	J0335+4555	16.6	—	101	J0613+3731	13.1	—
12	J0054+6946	15.7	—	57	J0335+6623	19	—	102	J0614+2229	16	67.6
13	J0056+4756	9.1	—	58	J0341+5711	14	—	103	J0614+83	7.3	—
14	J0058+4950	11.5	—	59	J0343+06	8.9	—	104	J0621+0336	32.1	—
15	J0058+6125	22.6	—	60	J0343+5312	13.9	—	105	J0624–0424	9.5	33.3
16	J0059+69	10.9	—	61	J0344–0901	29.5	—	106	J0627+0649	12.5	—
17	J0100+8023	12.5	—	62	J0357+5236	4.8	—	107	J0627+0706	32.3	—
18	J0102+6537	8.5	—	63	J0358+4155	8.9	—	108	J0629+2415	12.5	—
19	J0103+54	16.9	—	64	J0401–7608	12.1	—	109	J0630–0046	13.9	—
20	J0104+64	9.5	—	65	J0402+4825	3.5	—	110	J0636–23	10.6	—
21	J0107+1322	19.3	—	66	J0406+6138	10.9	—	111	J0636–4549	30.8	—
22	J0108+6608	13.3	—	67	J0408+552	5	—	112	J0645+80	7.3	—
23	J0108+6905	9.4	—	68	J0410–31	21.6	—	113	J0646+0905	12.5	—
24	J0108–1431	7.7	9.2	69	J0413+58	7.3	—	114	J0647+0913	23.1	—
25	J0110–22	11.2	—	70	J0414+31	12.7	—	115	J0652–0142	22.7	—
26	J0122+1416	18	—	71	J0415+6954	20	—	116	J0653+8051	16.6	—
27	J0125+62	15.7	—	72	J0417+35	21.9	—	117	J0656–2228	24.6	—
28	J0133–6957	15.6	—	73	J0417+61	7	—	118	J0656–5449	11.5	—
29	J0134–2937	12.6	—	74	J0418–4154	16.5	—	119	J0659–36	10.8	—
30	J0137+1654	4.1	—	75	J0421+3255	1	—	120	J0700+6418	12.5	—
31	J0137+6349	7.3	—	76	J0426+4933	19.3	—	121	J0709–5923	32.2	—
32	J0139+5621	15.7	—	77	J0448–2749	13	58.2	122	J0711+0931	16.6	—
33	J0139+5814	17.9	—	78	J0450–1248	7.4	—	123	J0719–2545	20.3	—
34	J0141+6009	6.7	—	79	J0452–1759	8.8	—	124	J0725–1635	26.5	—
35	J0147+5922	12.4	—	80	J0454+4529	16.3	—	125	J0733–2345	17.3	—
36	J0151–0635	5.5	—	81	J0454+5543	7.2	—	126	J0737–2202	7.1	—
37	J0152–1637	20.5	—	82	J0458–0505	26.8	—	127	J0738–4042	5.9	—
38	J0156+3949	6.3	—	83	J0459–0210	15.1	—	128	J0745–5353	4.5	25.5
39	J0201+7005	15.6	—	84	J0502+4654	10.3	—	129	J0747+6646	11.8	—
40	J0206–4028	19.9	—	85	J0517+2212	3.7	—	130	J0749–4247	23.7	—
41	J0210+5845	12.9	—	86	J0518+5416	10.5	—	131	J0750+57	6.4	—
42	J0211–8159	4.8	—	87	J0520–2553	11.7	—	132	J0754+3231	8.1	—
43	J0212+5222	11.5	—	88	J0525+1115	12.8	—	133	J0758–1528	39.3	80.2
44	J0215+6218	3.1	—	89	J0529–0715	15.5	—	134	J0758–30	12.5	—
45	J0231+7026	18.1	—	90	J0530–39	12.5	—	135	J0803–0942	21.9	—

Table 1. (Contd.)

No.	Name	β_1, deg	β_2, deg	No.	Name	β_1, deg	β_2, deg	No.	Name	β_1, deg	β_2, deg
136	J0807−5421	18.8	—	181	J0922−4949	21.4	—	226	J1046+0304	14.4	—
137	J0808−3937	16.9	—	182	J0924−5302	19.2	—	227	J1046−5813	16.3	—
138	J0809−4753	13.1	—	183	J0924−5814	5.3	17.7	228	J1047−3032	4.7	—
139	J0812−3905	6.2	—	184	J0930−2301	16.8	—	229	J1047−6709	11.5	—
140	J0814+7429	8.2	—	185	J0932−3217	26.8	—	230	J1048−5838	1.8	—
141	J0815+0939	2.1	—	186	J0934−4154	12.6	—	231	J1054−5943	37.3	—
142	J0815+4611	12.6	—	187	J0934−5249	19.6	—	232	J1054−5946	5	—
143	J0818−3049	5.3	—	188	J0941−5244	16.3	—	233	J1054−6452	31.3	—
144	J0820−1350	21	—	189	J0942−5552	8.5	—	234	J1055−6236	19.6	—
145	J0820−3826	6.3	—	190	J0942−5657	38.9	—	235	J1056−6258	7.1	—
146	J0820−3921	5.8	—	191	J0943+1631	4.3	—	236	J1057−7914	18.3	21.9
147	J0820−4114	1.9	—	192	J0944−1354	32.4	—	237	J1058−5957	17.6	—
148	J0821−4221	10.5	—	193	J0945−4833	18.8	—	238	J1059−5742	22.2	—
149	J0823+0159	15.3	—	194	J0947+2740	10.1	—	239	J1103−6025	28.1	—
150	J0826+2637	26.4	—	195	J0949−6902	25.9	—	240	J1104−6103	12.5	—
151	J0828−3417	1.2	—	196	J0952−3839	11.1	—	241	J1105−4353	9	—
152	J0831−4406	12.1	—	197	J0953+0755	7.5	—	242	J1107−5907	1.1	—
153	J0835−3707	30.7	—	198	J0954−5430	15.9	47.8	243	J1107−5947	10.6	—
154	J0836−4233	16.8	—	199	J0955−5304	16.8	—	244	J1107−6143	20.2	—
155	J0837+0610	21.6	—	200	J0957−5432	20.5	—	245	J1110+58	11.6	—
156	J0837−4135	25.1	—	201	J0959−4809	3.3	14.9	246	J1110−5637	11.9	—
157	J0838−2621	5.3	—	202	J1000−5149	18.6	—	247	J1112−6613	9.8	—
158	J0840−5332	13.3	—	203	J1001−5507	31.2	—	248	J1112−6926	13.7	—
159	J0842−4851	30.5	—	204	J1001−5559	17	—	249	J1114−6100	7.6	—
160	J0843−5022	12.1	10.6	205	J1002−5919	6.1	—	250	J1115+5030	27.2	—
161	J0846−3533	8.5	—	206	J1003−4747	11.2	—	251	J1115−6052	16.4	44.6
162	J0849+8028	9.6	—	207	J1006−6311	18.9	—	252	J1116−2444	14.9	—
163	J0849−6322	9.4	—	208	J1012−5857	22.1	—	253	J1116−4122	28.2	—
164	J0855−3331	25.4	—	209	J1013−5934	7.4	—	254	J1117−6154	11.7	—
165	J0855−4658	14.3	—	210	J1015−5719	1.6	—	255	J1120−24	23.5	—
166	J0856−6137	14.7	—	211	J1016−5345	29.2	—	256	J1121−5444	12.3	—
167	J0857−4424	11.2	—	212	J1017+3011	7	—	257	J1123−4844	11.8	40.6
168	J0901−4624	7.6	24.1	213	J1017−5621	23.8	38.1	258	J1123−6102	15.9	—
169	J0902−6325	14	—	214	J1018−1642	20.7	—	259	J1123−6259	12.1	60.4
170	J0904−4246	18.1	—	215	J1020−5921	21	—	260	J1123−6651	6.4	—
171	J0904−7459	10.9	33	216	J1020−6026	3.5	—	261	J1126−2737	11	—
172	J0905−4536	3	—	217	J1032−5911	16.6	—	262	J1126−38	8.9	—
173	J0905−5127	19.6	—	218	J1034−3224	2.2	—	263	J1126−6054	13.9	—
174	J0905−6019	16.2	—	219	J1035−6345	27.4	—	264	J1126−6942	13.8	—
175	J0907−5157	6.9	26.1	220	J1036−4926	18.2	—	265	J1130−5826	14.6	—
176	J0908−1739	11.1	—	221	J1036−6559	20.2	—	266	J1130−6807	2.6	—
177	J0909−7212	9.1	—	222	J1038−5831	18.8	—	267	J1132+25	23.6	—
178	J0912−3851	19.2	—	223	J1041−1942	12.6	55.6	268	J1132−4700	7.2	—
179	J0919−6040	15.8	—	224	J1042−5521	17.7	—	269	J1132−5627	18	—
180	J0921+6254	17.9	—	225	J1043−6116	15	—	270	J1133−6250	1.8	—

Table 1. (Contd.)

No.	Name	β_1, deg	β_2, deg	No.	Name	β_1, deg	β_2, deg	No.	Name	β_1, deg	β_2, deg
271	J1136−5525	8.6	—	316	J1252−6314	12	—	361	J1346−4918	10.3	—
272	J1136−6527	19.1	—	317	J1255−6131	20.8	—	362	J1347−5947	18.3	—
273	J1137−6700	2.8	—	318	J1255−62	1.9	—	363	J1349−6130	10.8	19.6
274	J1141−3107	12.4	—	319	J1257−1027	11.4	—	364	J1349−63	4.6	—
275	J1141−3322	8.2	—	320	J1259−6741	15.1	—	365	J1350−5115	25.1	—
276	J1142−6230	9	—	321	J1300−6602	6.8	—	366	J1352−6803	9.1	8.2
277	J1143−5158	22.6	—	322	J1305−6203	8.4	—	367	J1355−5153	30.5	—
278	J1143−5536	19.5	—	323	J1305−6455	6.9	—	368	J1355−5925	15.4	—
279	J1144−6217	16.1	—	324	J1306−6617	4.9	—	369	J1356−5521	9.8	—
280	J1146−6030	12.2	—	325	J1308−4650	9.8	—	370	J1357−62	6.5	—
281	J1152−6012	12.1	—	326	J1308−5844	22	—	371	J1358−2533	10.4	—
282	J1156−5707	10.5	14.7	327	J1311−1228	25.2	—	372	J1359−6038	15.5	—
283	J1156−5909	31.1	—	328	J1312−5402	10.7	—	373	J1401−6357	30	—
284	J1157−6224	6.4	—	329	J1312−5516	14.2	—	374	J1402−5021	12.6	—
285	J1159−6409	1.7	—	330	J1316−6232	1.3	—	375	J1403−6310	7.1	—
286	J1159−7910	15.8	—	331	J1317−6302	6.5	—	376	J1403−7646	10.7	—
287	J1202−5820	18.4	—	332	J1319−6056	14.8	—	377	J1405−5641	16.8	—
288	J1204−6843	16	—	333	J1319−6105	9.5	—	378	J1409−6953	10.2	—
289	J1210−5559	26.4	—	334	J1320+67	10.2	—	379	J1410−7404	65.7	—
290	J1210−6322	5.7	—	335	J1320−3512	9.2	—	380	J1412−6111	15.2	—
291	J1211−6324	11.9	—	336	J1320−5359	11.6	55.3	381	J1412−6145	6.1	—
292	J1214−5830	32.5	—	337	J1321+8323	10.4	—	382	J1413−6141	3.1	—
293	J1215−5328	7.2	—	338	J1321−5922	36.7	—	383	J1413−6222	3.3	—
294	J1220−6318	6	—	339	J1322−6241	23.9	—	384	J1413−6307	29.4	—
295	J1222−5738	39.1	—	340	J1326−5859	12.5	—	385	J1415−6621	17.2	—
296	J1223−5856	2.2	—	341	J1326−6408	10.8	—	386	J1416−5033	18.8	—
297	J1224−6208	16.7	—	342	J1326−6700	5.9	—	387	J1416−6037	9.6	—
298	J1225−5556	19.1	—	343	J1327−6222	17.8	—	388	J1418−3921	11.8	—
299	J1225−6035	53.5	—	344	J1327−6301	6.6	—	389	J1420−5416	18.2	—
300	J1225−6408	12.2	—	345	J1327−6400	1.6	—	390	J1423−6953	8.9	—
301	J1227−63	7.8	—	346	J1328−4357	17.9	—	391	J1424−5556	13.3	—
302	J1231−4609	9.6	—	347	J1328−4921	12.6	—	392	J1424−5822	10.7	44
303	J1232−4742	3	—	348	J1331−5245	8.9	—	393	J1424−6438	6.6	—
304	J1234−3630	16.3	—	349	J1332−3032	3.5	—	394	J1425−5723	18.3	—
305	J1235−54	5.4	—	350	J1333−4449	24.7	—	395	J1425−6210	19.1	—
306	J1236−5033	11.4	—	351	J1334−5839	11	—	396	J1427−4158	15.2	—
307	J1239+2453	14.8	—	352	J1335−3642	6.4	—	397	J1428−5530	15.5	—
308	J1239−6832	19.6	—	353	J1336−2522	12	—	398	J1430−5712	7.4	—
309	J1240−4124	34.1	—	354	J1338−6204	3.6	—	399	J1430−6623	19.4	—
310	J1243−5735	3.9	—	355	J1339−4712	19.2	—	400	J1434−5943	11	—
311	J1243−6423	30.9	—	356	J1339−6618	9.5	—	401	J1435−5954	8.4	43.9
312	J1244−6359	4.2	—	357	J1340−6456	11.6	—	402	J1439+7655	17.8	—
313	J1246+2253	18	—	358	J1341−6023	21	—	403	J1440−6344	13.3	—
314	J1248−6444	11.3	—	359	J1344−5855	6.6	—	404	J1443−5122	5.1	19.4
315	J1251−7407	20.7	—	360	J1345−6115	21.9	—	405	J1449−5846	10.4	—

Table 1. (Contd.)

No.	Name	β_1, deg	β_2, deg	No.	Name	β_1, deg	β_2, deg	No.	Name	β_1, deg	β_2, deg
406	J1452−6036	6.3	—	451	J1532−56	5.8	—	496	J1559−5545	23.5	—
407	J1453−6413	14.6	—	452	J1534−4428	3.9	—	497	J1600−5044	9.4	—
408	J1456−6843	6.3	—	453	J1534−5334	16.2	—	498	J1600−5751	5.4	—
409	J1457−5122	11.4	—	454	J1534−5405	9	—	499	J1600−5916	4.8	—
410	J1457−5902	17.2	—	455	J1535−4114	11.9	58.6	500	J1602−5100	19.5	—
411	J1501−0046	17.7	—	456	J1535−4415	2.2	—	501	J1603−2531	16.1	—
412	J1502+4653	24.3	—	457	J1535−5848	19.3	—	502	J1603−2712	14.3	—
413	J1502−5653	23.4	—	458	J1536−30	15.8	—	503	J1603−3539	6.1	—
414	J1502−6128	8.4	—	459	J1536−3602	7.7	—	504	J1603−5312	10.6	—
415	J1504−5621	12	—	460	J1536−5433	7.7	47.1	505	J1603−5657	45.1	—
416	J1504−5659	15.5	—	461	J1537−4912	5.8	—	506	J1604−4718	15.1	—
417	J1505−25	21.7	—	462	J1537−5153	19.3	—	507	J1604−4909	17	—
418	J1506−5158	14	—	463	J1538−5621	17.6	—	508	J1604−7203	6.4	—
419	J1507−4352	21.6	19.2	464	J1538−5732	17.7	—	509	J1605−5257	5	—
420	J1507−5800	8	—	465	J1538−5750	2.2	—	510	J1607−0032	15.1	—
421	J1507−6640	46.7	—	466	J1539−4828	16.5	—	511	J1607−6449	11.6	—
422	J1509+5531	16.6	—	467	J1539−5626	8	—	512	J1609−1930	34.3	—
423	J1510−4422	5.4	—	468	J1539−6322	11	—	513	J1609−4616	22.5	—
424	J1511−5414	18.4	—	469	J1540−5736	13.5	—	514	J1610−1322	6.5	—
425	J1511−5835	4.1	—	470	J1542−5034	34.1	—	515	J1610−5006	1.9	—
426	J1512−5759	5.6	—	471	J1542−5133	16.9	—	516	J1611−4949	6.9	—
427	J1513−5739	18.9	—	472	J1542−5303	9.7	—	517	J1611−5209	46.3	—
428	J1513−6013	17	—	473	J1543+0929	1.7	—	518	J1611−5847	39.7	—
429	J1514−4834	23.4	—	474	J1543−0620	25.1	—	519	J1612−2408	16.9	—
430	J1514−5316	11.4	—	475	J1543−5459	4.4	—	520	J1612−49	1.8	—
431	J1517−4356	17.6	—	476	J1544−5308	10.4	—	521	J1612−5022	15.4	—
432	J1517−4636	20	—	477	J1546−5302	19.4	—	522	J1612−55	8.7	—
433	J1518−0627	10.1	—	478	J1547−0944	20.8	—	523	J1612−5805	21.8	—
434	J1518−3952	5.4	—	479	J1547−5750	6.3	—	524	J1613−4714	16.8	16.1
435	J1519−5734	3.8	—	480	J1547−5839	3.6	—	525	J1614+0737	28.4	—
436	J1519−6308	18.4	—	481	J1548−4927	20.2	—	526	J1614−3846	6.3	—
437	J1522−5525	26.9	—	482	J1548−5607	5	—	527	J1614−3937	9.2	—
438	J1522−5829	8.9	—	483	J1549+2113	32.6	—	528	J1615−4958	5.4	—
439	J1523−3235	8.7	—	484	J1549−4848	15	55.3	529	J1615−5444	14.8	—
440	J1524−5706	16	—	485	J1550−5242	19.3	—	530	J1615−5537	21.3	—
441	J1525−5417	66.4	—	486	J1551−4424	5.2	—	531	J1616−5017	14.5	—
442	J1525−5523	5.3	–	487	J1551−6214	19.4	—	532	J1617−4608	20.2	—
443	J1527−5552	15.5	—	488	J1553−5456	4.8	—	533	J1618−4723	8.6	—
444	J1528−4109	23	41.7	489	J1555−0515	30.8	—	534	J1621−5039	14.8	—
445	J1529−26	15.1	—	490	J1555−2341	11.8	—	535	J1621−5243	6.5	—
446	J1530−21	10.5	—	491	J1555−3134	9.4	—	536	J1622−3751	8.9	—
447	J1530−5327	10.9	—	492	J1557−4258	12	—	537	J1622−4332	13	—
448	J1530−6343	17.7	—	493	J1557−5151	3.9	—	538	J1622−4347	18.6	—
449	J1531−4012	18.4	—	494	J1558−5756	30.3	—	539	J1622−4802	3.9	—
450	J1532+2745	18.2	—	495	J1559−4438	9.5	—	540	J1622−4845	10.2	—

Table 1. (Contd.)

No.	Name	β_1, deg	β_2, deg	No.	Name	β_1, deg	β_2, deg	No.	Name	β_1, deg	β_2, deg
541	J1623−0908	41.3	—	586	J1639−4604	9.7	—	631	J1658−4958	9.4	—
542	J1623−4256	7.7	—	587	J1640−4715	3.8	—	632	J1659−1305	5.6	—
543	J1623−4949	13.8	—	588	J1641−2347	6.9	16.8	633	J1700−3312	15.7	—
544	J1624+5850	14.3	—	589	J1643+1338	20.6	—	634	J1700−3611	14	29.8
545	J1624+8643	20.4	—	590	J1643−4505	7.8	—	635	J1700−4012	6.5	—
546	J1624−4411	2.9	—	591	J1643−4550	15.1	—	636	J1700−4422	6.1	—
547	J1624−4613	2.6	—	592	J1644−33	4.3	—	637	J1700−4939	4.4	—
548	J1625−4913	9.5	—	593	J1644−4559	21	—	638	J1701−3130	10.6	—
549	J1626−4537	9.4	—	594	J1645+1012	12.5	—	639	J1701−4533	4.7	—
550	J1626−6621	12.4	—	595	J1645−0317	31.3	—	640	J1702−4310	6.6	16.3
551	J1627+1419	7.4	—	596	J1646−5123	13.3	—	641	J1703−1846	20.7	—
552	J1627−4706	4	—	597	J1646−6831	10.1	—	642	J1703−3241	14.1	—
553	J1627−4845	2.2	—	598	J1647+6608	16.4	—	643	J1703−4442	17.5	—
554	J1627−49	3.8	—	599	J1647−3607	9	—	644	J1703−4851	14.4	—
555	J1627−51	16.5	—	600	J1648−3256	25.5	—	645	J1704−3756	8.9	—
556	J1627−5547	9	—	601	J1648−6044	12.9	—	646	J1704−5236	6	—
557	J1627−5936	1.9	—	602	J1649+2533	15.4	—	647	J1704−6016	1.6	—
558	J1628−4804	2	—	603	J1649−3805	5.1	—	648	J1705−3423	7.6	—
559	J1629+33	14.3	—	604	J1649−3935	9.9	—	649	J1705−3950	5.8	—
560	J1629+43	7.7	—	605	J1649−4349	2.7	—	650	J1705−4331	9.4	—
561	J1629−3825	23	—	606	J1650−1654	15.8	—	651	J1705−6135	5.5	—
562	J1630−4719	17.7	—	607	J1650−4126	14.8	—	652	J1706+59	14.9	—
563	J1631−4155	11.8	—	608	J1650−4502	12.3	32.8	653	J1706−4434	12.1	—
564	J1632−1013	12.4	—	609	J1651−1709	16.6	—	654	J1706−6118	46.5	—
565	J1632−4621	23.1	—	610	J1651−4246	3.3	12.6	655	J1707−4053	4.4	—
566	J1633−4453	8.8	—	611	J1651−5222	17.2	—	656	J1707−4341	18.6	—
567	J1633−5015	10.3	—	612	J1651−5255	7.9	—	657	J1707−4729	4	—
568	J1634−49	6.4	—	613	J1651−7642	9.3	45.4	658	J1708−3426	11.6	—
569	J1634−5107	7.8	—	614	J1652+2651	11	—	659	J1708−3641	4.5	—
570	J1634−5640	8.8	—	615	J1652−1400	8.2	36.7	660	J1708−4522	20.1	—
571	J1635+2418	16.2	—	616	J1652−2404	18.4	—	661	J1708−7539	15.1	—
572	J1635−1511	2.6	—	617	J1653−3838	13.5	—	662	J1709−1640	20.6	—
573	J1635−4944	4.2	—	618	J1653−4030	3.7	—	663	J1709−3626	8.2	—
574	J1635−5954	9.6	—	619	J1653−4105	6.7	—	664	J1709−4401	25.8	—
575	J1636−2614	24.1	—	620	J1653−4249	10.4	—	665	J1710−2616	5.7	9.2
576	J1637−4450	1.6	—	621	J1653−45	19.1	—	666	J1710−37	4.4	—
577	J1637−4553	13.3	—	622	J1654−2636	6	—	667	J1711−1509	25.9	—
578	J1638+4005	15.2	—	623	J1654−2713	14.5	—	668	J1711−4322	4.3	—
579	J1638−35	13	—	624	J1654−3710	17.1	—	669	J1711−5350	23.1	—
580	J1638−3815	5.9	—	625	J1655−3048	3	—	670	J1712−2715	2.5	—
581	J1638−4233	7	—	626	J1656+6203	15	—	671	J1713+7810	10.9	—
582	J1638−44	6.7	—	627	J1656−3621	11.9	—	672	J1714−1054	5	—
583	J1638−4725	3.4	—	628	J1657+3304	17.8	—	673	J1715−3859	4.2	—
584	J1638−5226	7.2	—	629	J1657−4432	11.7	—	674	J1716−3720	3.6	—
585	J1639−4359	10	—	630	J1658−47	5.2	—	675	J1716−4111	18.2	—

Table 1. (Contd.)

No.	Name	β_1, deg	β_2, deg	No.	Name	β_1, deg	β_2, deg	No.	Name	β_1, deg	β_2, deg
676	J1716−4711	21.1	—	721	J1733−2533	6.8	—	766	J1745+1252	5.8	—
677	J1717−3425	9.7	—	722	J1733−2837	22.9	—	767	J1745−0129	33.2	—
678	J1717−3737	5.9	—	723	J1733−3716	3.7	—	768	J1745−2758	6.9	—
679	J1717−3953	1.8	—	724	J1733−4005	20	—	769	J1745−3040	10.7	—
680	J1717−4054	39.6	—	725	J1733−5515	8.4	51	770	J1745−3812	17.3	—
681	J1717−5800	6.6	—	726	J1734−0212	11.7	—	771	J1746+2540	18.6	—
682	J1718−41	4.7	—	727	J1734−2415	7.4	—	772	J1748−1300	12	—
683	J1718−4539	9.7	—	728	J1734−2859	7	—	773	J1748−30	3	—
684	J1719−2330	15.3	—	729	J1734−3058	14.4	—	774	J1749+5952	10.1	—
685	J1719−3458	11.5	—	730	J1735−0243	4.3	—	775	J1749−3002	4.1	—
686	J1719−4006	8.6	36.2	731	J1735−0724	11.6	—	776	J1749−4931	35.8	—
687	J1719−4302	18	—	732	J1737−3102	14.6	—	777	J1749−5417	8.6	—
688	J1720+2150	12.9	—	733	J1737−3555	15.2	—	778	J1749−5605	11.6	—
689	J1720−0212	3.5	—	734	J1738−2330	15.9	—	779	J1750−2438	22.5	—
690	J1720−1633	19.3	—	735	J1738−2736	15.8	—	780	J1750−28	21.3	—
691	J1720−2446	9	—	736	J1738−2955	4.3	—	781	J1750−3157	6.2	—
692	J1720−2933	10.8	79.9	737	J1738−3211	18.2	—	782	J1750−3503	3.6	—
693	J1720−3659	10.3	—	738	J1739+0612	9.8	—	783	J1751−3323	9.6	—
694	J1721−3532	2.6	—	739	J1739−1313	86.2	—	784	J1751−4657	22.2	—
695	J1722+35	9.4	—	740	J1739−2903	20.2	—	785	J1752+2359	23.1	—
696	J1722−3207	14.4	—	741	J1739−3131	3.3	—	786	J1752−2806	29	—
697	J1722−3632	6.2	—	742	J1739−3951	11.1	—	787	J1752−2821	19.2	—
698	J1722−3712	15.4	—	743	J1740+1311	9.7	—	788	J1753−2501	3.4	—
699	J1722−4400	20	—	744	J1740+27	16.5	—	789	J1753−38	18.1	—
700	J1723−3659	7.6	16.9	745	J1740−3015	38.6	—	790	J1754−3443	11.7	—
701	J1723−38	12.8	—	746	J1740−3327	13.5	—	791	J1754−3510	20.2	—
702	J1724−4500	19.7	—	747	J1741+2758	19.4	—	792	J1755−0903	12.6	—
703	J1725−0732	7.5	—	748	J1741+3855	12.5	—	793	J1755−1650	16.7	—
704	J1725−2852	9	—	749	J1741−2719	7.1	—	794	J1755−2521	20.6	—
705	J1725−3546	6.1	—	750	J1741−2733	9.4	—	795	J1755−2550	7.6	—
706	J1725−4043	8.3	—	751	J1741−3016	9.4	—	796	J1755−26	10.2	—
707	J1726−3635	2.7	—	752	J1741−34	11.7	—	797	J1755−2725	5.8	—
708	J1727−2739	6.5	—	753	J1741−3927	12.3	—	798	J1756−2435	10.1	—
709	J1728−0007	7.6	—	754	J1742−0203	8.6	—	799	J1756−25	13.1	—
710	J1728−3733	20.6	—	755	J1742−3957	4.9	—	800	J1757−1500	24.6	—
711	J1728−4028	4.2	—	756	J1742−4616	6.8	29.2	801	J1757−2223	24.2	—
712	J1730−2900	19.8	—	757	J1743−0339	15	—	802	J1758+3030	13	—
713	J1731−33	4.1	—	758	J1743−1351	9.9	—	803	J1758−2846	15	—
714	J1731−3322	4.6	—	759	J1743−35	10	—	804	J1759−1736	10.6	—
715	J1732−1930	12.7	—	760	J1743−4212	12.7	—	805	J1759−2205	26	—
716	J1732−3426	6.2	—	761	J1744−1610	24.4	—	806	J1759−2307	6.4	—
717	J1732−35	5.9	—	762	J1744−2335	16	—	807	J1759−24	5.1	—
718	J1732−4128	15.6	—	763	J1744−3130	22.2	—	808	J1759−2922	17.2	—
719	J1733−01	11.7	—	764	J1744−3922	18	—	809	J1759−3107	26.5	—
720	J1733−2228	6	—	765	J1744−5337	5.2	—	810	J1800+5034	17.4	—

Table 1. (Contd.)

No.	Name	β_1, deg	β_2, deg	No.	Name	β_1, deg	β_2, deg	No.	Name	β_1, deg	β_2, deg
811	J1800−0125	9	—	856	J1812−2526	10.3	—	901	J1824−0132	6.3	—
812	J1801−0357	16.3	—	857	J1812−3039	14.6	—	902	J1824−1118	5.2	—
813	J1801−2920	10.1	—	858	J1813+1822	10.4	—	903	J1824−1350	13.6	—
814	J1801−3458	7.1	—	859	J1813+4013	19.5	—	904	J1824−1423	7.9	—
815	J1802+0128	15.1	—	860	J1813−2113	11.3	—	905	J1824−1945	39.4	—
816	J1802−0523	6.4	—	861	J1814−0521	13.6	—	906	J1824−2233	21	—
817	J1803−2712	6.4	32.6	862	J1814−0618	4	—	907	J1824−2328	16.7	—
818	J1803−3329	18	—	863	J1814−1649	9.5	—	908	J1825+0004	13.8	—
819	J1804−28	10.8	—	864	J1815+5546	14.4	—	909	J1825−1108	15.5	—
820	J1805+0306	11.5	—	865	J1815−1910	13.7	—	910	J1825−1446	6.2	—
821	J1805−0619	10.2	—	866	J1816−1729	12.4	73.5	911	J1827−0750	4.5	—
822	J1805−1504	2	11.1	867	J1816−2650	5.4	—	912	J1827−0958	2.7	—
823	J1805−2447	17.9	—	868	J1816−5643	6.1	—	913	J1828−0611	9.9	—
824	J1805−2948	11.8	—	869	J1817−0743	7.8	—	914	J1828−2119	9.1	—
825	J1806−1154	8	—	870	J1817−3618	13.9	—	915	J1829+0000	6	—
826	J1806−2125	5.3	—	871	J1817−3837	24	—	916	J1829−0734	10.3	—
827	J1807+0756	10.4	—	872	J1818−0151	13.9	—	917	J1829−1011	3.9	—
828	J1807−0847	8.8	—	873	J1818−1422	3.4	—	918	J1829−1751	10.6	—
829	J1807−2715	19.5	—	874	J1819+1305	7.4	—	919	J1830−0052	13.3	—
830	J1808+00	7.6	—	875	J1819−0925	15.1	—	920	J1830−0131	5.5	—
831	J1808−0813	13.4	—	876	J1819−1114	2.5	—	921	J1830−10	12.1	—
832	J1808−1020	13.7	—	877	J1819−1318	21.1	—	922	J1830−1059	26.7	41.5
833	J1808−1517	18.3	—	878	J1819−1510	4.8	—	923	J1830−1414	20.8	—
834	J1808−2057	6.3	—	879	J1819−37	9.6	—	924	J1831−04	22.1	—
835	J1808−3249	12.4	—	880	J1820−0427	18.9	—	925	J1831−0823	18.3	—
836	J1809−0119	19.2	—	881	J1820−0509	9.9	—	926	J1832+0029	21.7	—
837	J1809−0743	10.8	—	882	J1820−1346	3.5	—	927	J1832−0644	7.3	—
838	J1809−1429	21.1	—	883	J1820−1818	6.8	—	928	J1832−0827	16.8	—
839	J1809−2109	28.5	—	884	J1821+1715	12.1	—	929	J1832−1021	8.5	38.7
840	J1809−3547	2.7	—	885	J1821+4147	16.4	—	930	J1833−0209	5.9	—
841	J1810+0705	1.6	—	886	J1821−0256	10.1	—	931	J1833−0338	21.7	—
842	J1810−1709	2.2	—	887	J1821−1432	10.9	—	932	J1833−6023	13.1	—
843	J1810−1820	3.2	—	888	J1822+02	9.1	—	933	J1834−0010	9	—
844	J1810−5338	7.4	—	889	J1822+1120	16.9	—	934	J1834−0031	15.7	—
845	J1811−0154	15.4	—	890	J1822+2617	27.3	—	935	J1834−0426	1.8	—
846	J1811−1717	4.1	—	891	J1822−0719	16.3	—	936	J1834−0602	8.4	—
847	J1811−1736	1.3	—	892	J1822−0848	8.8	—	937	J1834−0731	2.3	—
848	J1811−2439	10.5	—	893	J1822−0902	13.6	—	938	J1834−09	2.1	—
849	J1811−4930	21	—	894	J1822−1400	8	—	939	J1834−1202	4.8	—
850	J1812+0226	23.7	—	895	J1822−2256	12.8	34.3	940	J1834−1710	10.5	—
851	J1812−15	17.2	—	896	J1822−4209	9.8	—	941	J1834−1855	11.6	—
852	J1812−1718	11.4	—	897	J1823+0550	7.3	—	942	J1835−0349	17.6	—
853	J1812−1733	1.8	—	898	J1823−0154	30.9	—	943	J1835−0643	3.2	—
854	J1812−20	2.7	—	899	J1823−1126	23.8	—	944	J1835−0847	4.6	—
855	J1812−2102	10.5	74.4	900	J1823−3106	20.1	44.6	945	J1835−09242	3.3	—

Table 1. (Contd.)

No.	Name	β_1, deg	β_2, deg	No.	Name	β_1, deg	β_2, deg	No.	Name	β_1, deg	β_2, deg
946	J1835−0928	5.7	—	991	J1842−0415	11.7	—	1036	J1851+1259	36.4	—
947	J1835−0944	5	—	992	J1842−0800	13.7	—	1037	J1851−0029	9.7	—
948	J1835−0946	33.9	—	993	J1842−0905	10.6	—	1038	J1851−0053	24.6	—
949	J1835−1020	17.2	—	994	J1842−39	4	—	1039	J1851−0114	12.5	—
950	J1835−1106	12.7	44.3	995	J1843−0000	13.5	69.8	1040	J1851−0633	19.5	—
951	J1835−1548	9.4	—	996	J1843−0459	4.9	—	1041	J1852−0118	5.7	—
952	J1836+51	11.6	—	997	J1843−0510	11	—	1042	J1852−0127	3.2	—
953	J1836−0436	12.1	—	998	J1843−0702	17.4	—	1043	J1852−0635	2.8	—
954	J1836−1008	20	—	999	J1843−1507	18.5	—	1044	J1852−2610	7.4	—
955	J1836−11	5.4	—	1000	J1844+00	6.5	—	1045	J1853+0011	11.7	25.1
956	J1836−1324	7.1	—	1001	J1844+1454	14.4	—	1046	J1853+0505	2.7	—
957	J1837+0053	2.7	—	1002	J1844−0030	12.2	—	1047	J1853+0545	3.2	—
958	J1837+1221	24.1	—	1003	J1844−0244	6.6	—	1048	J1854+36	5.2	—
959	J1837−0045	11.8	—	1004	J1844−0302	20.8	—	1049	J1854−0524	14	—
960	J1837−0653	5.8	—	1005	J1844−0433	21.5	—	1050	J1854−1421	14	—
961	J1837−0822	11.7	—	1006	J1844−0538	7	—	1051	J1855+0307	19.1	—
962	J1837−1837	19.5	—	1007	J1845+0623	32.2	—	1052	J1855−0941	4.7	—
963	J1838+1523	4.9	—	1008	J1845−0434	11.7	—	1053	J1856+0102	13.4	—
964	J1838+1650	11.4	—	1009	J1845−0545	19.2	—	1054	J1856−0526	5.7	—
965	J1838−0107	6	—	1010	J1845−0635	8.4	—	1055	J1857+0057	6.1	—
966	J1838−1046	20.7	—	1011	J1845−0743	7.4	—	1056	J1857+0143	2.2	—
967	J1839−0223	10.6	—	1012	J1845−0826	12.1	—	1057	J1857+0212	10.5	—
968	J1839−0402	19.8	—	1013	J1845−1114	23.9	—	1058	J1857+0526	7.2	—
969	J1839−0436	8.1	—	1014	J1846+0051	11	—	1059	J1859+00	3.5	—
970	J1839−0627	10.1	—	1015	J1846−0749	12.7	—	1060	J1859+1526	17	—
971	J1839−0643	3.7	—	1016	J1846−07492	13.9	—	1061	J1859+7654	15.5	—
972	J1839−1238	21.9	—	1017	J1847−0402	12.3	—	1062	J1900+0634	11.7	—
973	J1840+0214	21.5	—	1018	J1847−0427	3.4	—	1063	J1900+30	18.1	—
974	J1840+5640	16.1	—	1019	J1847−0438	27.1	—	1064	J1900−0051	16.9	—
975	J1840−0445	4.8	—	1020	J1847−0605	12.3	—	1065	J1900−0134	17.8	—
976	J1840−0559	11.1	—	1021	J1848+0647	11.3	—	1066	J1900−0933	3.2	—
977	J1840−0809	15.9	—	1022	J1848+0826	5.5	—	1067	J1900−2600	5.6	—
978	J1840−0815	18.7	—	1023	J1848−0023	13.4	—	1068	J1900−7951	8.5	—
979	J1840−1207	21.4	—	1024	J1848−0123	10.5	—	1069	J1901+0156	12.8	—
980	J1841+0912	16.8	—	1025	J1848−0601	6.4	—	1070	J1901+0331	11.1	—
981	J1841−0157	9.8	—	1026	J1848−1150	17.8	—	1071	J1901+0716	9.5	—
982	J1841−0345	6.5	26.9	1027	J1848−1414	6.2	—	1072	J1901+1306	15.5	—
983	J1841−0425	12.2	31.6	1028	J1849+0409	28.8	—	1073	J1901−0312	4.6	—
984	J1841−1404	6.2	—	1029	J1849+2423	6.4	—	1074	J1901−0315	23.9	—
985	J1841−7845	5.2	—	1030	J1849−0317	11.3	—	1075	J1901−0906	17.8	—
986	J1842+0358	18.6	—	1031	J1849−0614	18.5	—	1076	J1901−1740	9	—
987	J1842+0638	9.7	—	1032	J1849−0636	32.9	—	1077	J1902+0556	15.7	—
988	J1842+1332	2	—	1033	J1850+0026	6.3	—	1078	J1902+0615	32	—
989	J1842−0153	9.1	—	1034	J1850+1335	17.9	64.3	1079	J1902+0723	5.2	—
990	J1842−0359	3	15.6	1035	J1850−0026	2	—	1080	J1902−1036	24.8	—

Table 1. (Contd.)

No.	Name	β_1, deg	β_2, deg	No.	Name	β_1, deg	β_2, deg	No.	Name	β_1, deg	β_2, deg
1081	J1903+0135	23	—	1126	J1912+1036	8.3	—	1171	J1923+4243	13.1	—
1082	J1903+2225	14.9	—	1127	J1912+2525	23.5	—	1172	J1924+2040	5.3	—
1083	J1903–0258	5.5	—	1128	J1913+0446	15.1	—	1173	J1925+19	8.1	—
1084	J1903–0632	16.5	—	1129	J1913+0936	13.9	—	1174	J1926+0431	23.3	—
1085	J1903–0848	14.3	—	1130	J1913+1000	7.8	—	1175	J1926+1434	5	—
1086	J1904+0004	6	12.5	1131	J1913+1145	6.8	—	1176	J1926+1648	18.4	—
1087	J1904+1011	6	—	1132	J1913+1400	15.7	—	1177	J1926+1928	8.6	—
1088	J1904+33	7.7	—	1133	J1913+3732	16.6	—	1178	J1926–0652	3.6	—
1089	J1904–0150	18	—	1134	J1913–0440	27.6	—	1179	J1927+0911	25	—
1090	J1904–1224	17.8	—	1135	J1914+0219	12.6	68.4	1180	J1927+1852	10.4	—
1091	J1904–1629	29.1	—	1136	J1914+0631	15.4	—	1181	J1927+1856	4.3	—
1092	J1905+0600	7.6	—	1137	J1914+1122	15.6	—	1182	J1927+2234	9.6	—
1093	J1905+0616	28.1	—	1138	J1915+0227	7	—	1183	J1928+1923	5	—
1094	J1905+0709	6.1	—	1139	J1915+0738	48.5	—	1184	J1928+28	10.9	—
1095	J1905–0056	48.5	—	1140	J1915+0838	8.4	—	1185	J1929+00	12.3	—
1096	J1906+0641	6.2	—	1141	J1915+1009	26.7	—	1186	J1929+1844	14.2	—
1097	J1906+0649	12.2	—	1142	J1915+1410	7.7	—	1187	J1929+1955	10.1	—
1098	J1906+0746	72.4	—	1143	J1915+1647	19.4	—	1188	J1929+2121	27.4	—
1099	J1906+1854	6.3	—	1144	J1916+0748	1.5	—	1189	J1929+3817	5.6	—
1100	J1907+0249	6.7	—	1145	J1916+0844	9.2	—	1190	J1929+62	17.2	—
1101	J1907+0731	13.1	—	1146	J1916+0951	14.1	—	1191	J1929+66	12.4	—
1102	J1907+0740	16.4	—	1147	J1916+1030	9.5	—	1192	J1930+1316	21.5	—
1103	J1907+0918	36.1	—	1148	J1916+1312	18.5	—	1193	J1930–1852	13.1	—
1104	J1907+1149	29.7	—	1149	J1916+3224	14	—	1194	J1931+1536	7.2	—
1105	J1907+1247	14.7	—	1150	J1916–2939	11.6	—	1195	J1931+1952	21.9	—
1106	J1907+4002	9.7	—	1151	J1917+1353	14.8	58.7	1196	J1931+30	15.8	—
1107	J1907+57	10.3	—	1152	J1917+2224	6.8	—	1197	J1931–0144	8.7	—
1108	J1908+0457	8.3	—	1153	J1918+1444	25.6	—	1198	J1932+1059	11.9	21.3
1109	J1908+0500	35.5	—	1154	J1918+1541	8.9	—	1199	J1932+2020	4.2	—
1110	J1908+0734	7.5	—	1155	J1918–1052	23.8	—	1200	J1932–3655	16.3	—
1111	J1908+0909	11.5	—	1156	J1919+0021	20.3	—	1201	J1933+0758	18.3	—
1112	J1908+0916	5.1	—	1157	J1919+0134	11.2	—	1202	J1933+1304	17.5	—
1113	J1908+2351	16.6	—	1158	J1919+2621	21	—	1203	J1933+2421	11.6	—
1114	J1909+0007	28.8	—	1159	J1920+2650	16.4	—	1204	J1934+2352	10.1	—
1115	J1909+0254	17.4	—	1160	J1920–0950	9.9	—	1205	J1934+5219	7.5	—
1116	J1909+0749	14	—	1161	J1921+0812	41.4	—	1206	J1935+1159	3.8	—
1117	J1909+1102	16.2	—	1162	J1921+1419	9.2	—	1207	J1935+1616	24.8	—
1118	J1909+1450	6.7	—	1163	J1921+1948	3.6	—	1208	J1935+1745	26.5	—
1119	J1909+1859	11.6	—	1164	J1921+2003	9.5	—	1209	J1937+2544	6.4	—
1120	J1910+0225	6.9	—	1165	J1921+2153	17.7	—	1210	J1937+2950	7.7	—
1121	J1910+0728	10	—	1166	J1922+1733	12.4	—	1211	J1938+0650	31.9	—
1122	J1910+1231	19.6	—	1167	J1922+2018	8.3	—	1212	J1938+2213	8.9	—
1123	J1910–0112	8.6	—	1168	J1922+2110	19.1	—	1213	J1939+2449	11.2	—
1124	J1910–0309	12.1	—	1169	J1922+58	16	—	1214	J1940+0239	11.7	—
1125	J1911+1758	13.9	—	1170	J1923+1706	11.7	—	1215	J1940–2403	14.7	—

Table 1. (Contd.)

No.	Name	β_1, deg	β_2, deg	No.	Name	β_1, deg	β_2, deg	No.	Name	β_1, deg	β_2, deg
1216	J1941+0121	4.1	—	1261	J2013+3845	3.6	—	1306	J2116+1414	12.1	—
1217	J1941+1026	17	—	1262	J2013−0649	14.4	—	1307	J2122+2426	7.9	—
1218	J1941+1341	10.1	—	1263	J2017+2043	15.4	—	1308	J2123+36	18.5	—
1219	J1941+4320	16.4	—	1264	J2017+5906	3.6	—	1309	J2123+5434	12.9	—
1220	J1941−2602	22.7	—	1265	J2017−2737	2.3	—	1310	J2124+1407	14.1	—
1221	J1942+1743	4.5	—	1266	J2018+2839	15.1	—	1311	J2127−6648	5.9	—
1222	J1942+3941	6.7	—	1267	J2019+72	2.5	—	1312	J2129+4119	15.1	—
1223	J1942+8106	21.9	—	1268	J2022+2854	13.4	—	1313	J2136−1606	11.2	—
1224	J1943+0609	12.9	—	1269	J2022+5154	10.8	—	1314	J2137+6428	18.2	—
1225	J1943−1237	26.2	—	1270	J2023+5037	15.4	—	1315	J2138+4911	6.9	—
1226	J1944+1755	5.8	—	1271	J2027+2146	11.6	—	1316	J2139+00	6	—
1227	J1944−1750	16.1	—	1272	J2027+4557	5.2	—	1317	J2139+2242	13	—
1228	J1945+1834	12.5	—	1273	J2027+7502	3.5	—	1318	J2145+21	17.9	—
1229	J1945−0040	8.1	—	1274	J2029+3744	15.9	—	1319	J2148−34	15	—
1230	J1946+1805	5.2	—	1275	J2030+2228	12.5	—	1320	J2149+6329	6.6	—
1231	J1946+2244	20.7	—	1276	J2030+55	9.8	—	1321	J2150+5247	8.2	—
1232	J1946−1312	15.7	—	1277	J2033−1938	15.2	—	1322	J2151+2315	5.2	—
1233	J1946−2913	24.6	—	1278	J2036+2835	21.7	—	1323	J2154−2812	38.8	—
1234	J1947+0915	14.1	—	1279	J2036+6646	9.5	—	1324	J2155+2813	21.8	—
1235	J1947−4215	11.1	—	1280	J2037+3621	7.5	—	1325	J2155−3118	19.3	—
1236	J1948+3540	8.4	—	1281	J2038+35	8.6	—	1326	J2155−5641	8.6	—
1237	J1948−27	18.8	—	1282	J2038+5319	14.9	—	1327	J2156+2618	17.8	—
1238	J1949+3426	4.5	—	1283	J2038−3816	21.3	—	1328	J2157+4017	7.5	—
1239	J1949−2524	27.1	—	1284	J2040+1657	6.3	—	1329	J2158−27	11.1	—
1240	J1951+4724	1.7	—	1285	J2040−21	11.2	—	1330	J2203+50	6	—
1241	J1953+1149	21.9	—	1286	J2043+7045	14.6	—	1331	J2205+1444	9.3	—
1242	J1953+2732	17.3	—	1287	J2044+28	15.4	—	1332	J2206+6151	4.1	—
1243	J1954+2923	14.7	—	1288	J2044+4614	3.7	—	1333	J2207−15	11.2	—
1244	J1954+3852	22.1	—	1289	J2045+0912	8.9	—	1334	J2208+5500	18.2	—
1245	J1954+4357	5.7	—	1290	J2046+1540	13	—	1335	J2209+22	24.6	—
1246	J1955+5059	24.1	—	1291	J2046+5708	11.6	—	1336	J2212+2933	9.8	—
1247	J1956+0838	7	—	1292	J2046−0421	25.9	—	1337	J2215+1538	29.7	—
1248	J1957−0002	19.9	—	1293	J2048+2255	9.8	—	1338	J2217+5733	6	—
1249	J2001+4258	21.5	—	1294	J2048−1616	12.9	—	1339	J2219+4754	25.2	—
1250	J2002+1637	10.8	—	1295	J2053−7200	5.8	26.9	1340	J2222+2923	8	—
1251	J2002+30	3.3	—	1296	J2054−39	15.3	—	1341	J2222+5602	6.2	—
1252	J2002+3217	10.1	—	1297	J2055+2209	21.1	—	1342	J2227+30	15.4	—
1253	J2002+4050	11.2	—	1298	J2055+3630	8.3	—	1343	J2228+6447	14	—
1254	J2006+4058	15.9	—	1299	J2102+38	10.3	—	1344	J2229+6205	7.6	—
1255	J2006−0807	3.6	—	1300	J2105+28	20.9	—	1345	J2234+2114	2.8	—
1256	J2007+0910	21.7	—	1301	J2108+4441	2.5	—	1346	J2241+6941	45.9	—
1257	J2008+2513	10.9	—	1302	J2108−3429	33.7	—	1347	J2242+6950	16.7	—
1258	J2010+2845	14.7	—	1303	J2113+2754	30.2	—	1348	J2243+1518	12.2	—
1259	J2012−2029	9.8	—	1304	J2113+4644	3.8	—	1349	J2244+63	12.1	—
1260	J2013+3058	25.2	—	1305	J2113+67	11.8	—	1350	J2248−0101	17	—

Table 1. (Contd.)

No.	Name	β_1, deg	β_2, deg	No.	Name	β_1, deg	β_2, deg	No.	Name	β_1, deg	β_2, deg
1351	J2251+24	11.7	—	1362	J2315+58	11.3	—	1372	J2333+6145	4.6	—
1352	J2253+1516	10	—	1363	J2317+2149	24.5	—	1373	J2338+4818	9.3	—
1353	J2257+5909	7	—	1364	J2319+6411	1.8	—	1374	J2343+6221	10.2	—
1354	J2257–16	26.5	—	1365	J2325+6316	5.4	—	1375	J2346–0609	11	59.7
1355	J2302+6028	19.3	—	1366	J2325–0530	19.6	—	1376	J2347+02	19.8	—
1356	J2305+3100	26.6	—	1367	J2326+6113	6.4	—	1377	J2351+8533	17.8	—
1357	J2305+4707	10.2	—	1368	J2326+6141	10	—	1378	J2352+65	5.6	—
1358	J2307+2225	15.3	—	1369	J2327+62	6.4	—	1379	J2354+6155	14.8	—
1359	J2308+5547	8.3	—	1370	J2329+4743	25.8	—	1380	J2354–22	16	—
1360	J2312+6931	14.9	—	1371	J2330–2005	29.8	—	1381	J2355+2246	8.9	—
1361	J2313+4253	14.8	—								

where N_1 and N_2 are the numbers of pulsars in the first and second samples. The value of the Kolmogorov quantile $\lambda = 2.98$ calculated according to (18) means that the β_1 samples for pulsars with $0.1 < P < 2$ s and $P > 2$ s are statistically different with a probability $p = 0.99999$.

The resulting distributions can be fitted by Gaussians (Figs. 6, 7)

$$\frac{n}{N(\beta_1)} = (0.492 \pm 0.010) \times \exp\left\{-\frac{(\beta_1 - (16.0 \pm 0.2))^2}{2(8.7 \pm 0.4)^2}\right\} \quad (19)$$

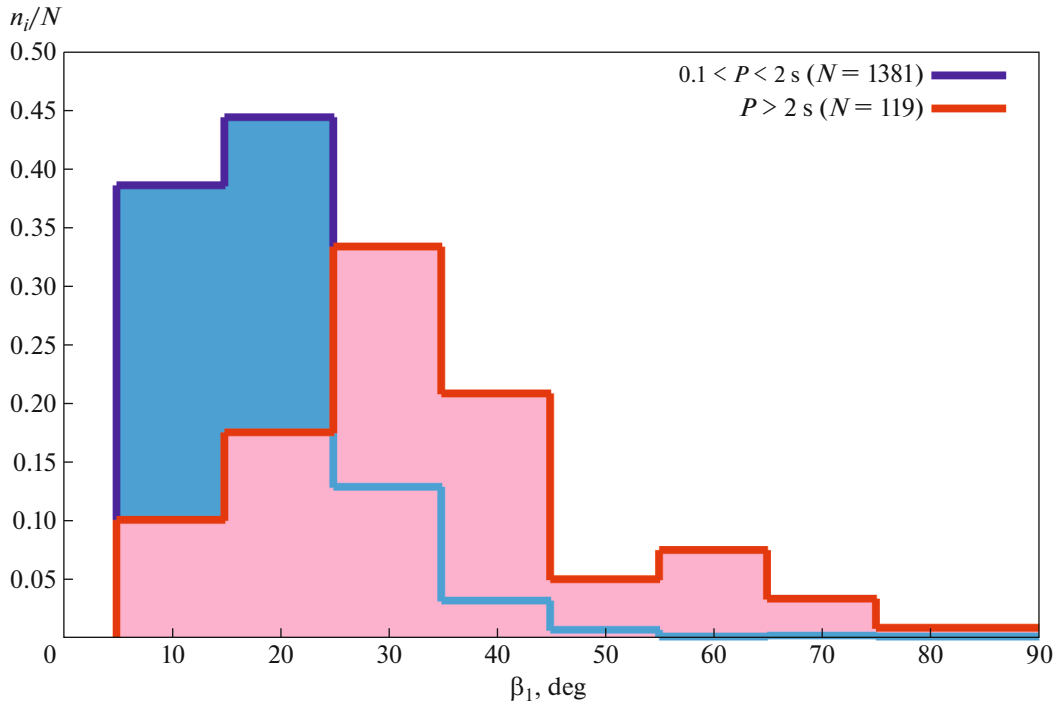

Fig. 5. Angle β_1 distribution histograms for the pulsar samples with $0.1 < P < 2$ s and $P > 2$ s normalized to the number N of pulsars in the sample.

Table 2. Angle β values for the sample of pulsars with periods $P > 2$ s

No.	Name	β_1, deg	β_2, deg	No.	Name	β_1, deg	β_2, deg	No.	Name	β_1, deg	β_2, deg
1	J0021−0909	51.8	—	41	J1404+1159	36.3	—	81	J1839−0332	34.1	—
2	J0055+5117	20.6	—	42	J1414−6802	14.8	—	82	J1840−0840	8	—
3	J0111+6624	30	—	43	J1432−5032	2.9	—	83	J1842+0257	23.8	—
4	J0152+0948	20.5	—	44	J1444−5941	27.2	—	84	J1843−0211	18.3	—
5	J0157+6212	16.5	—	45	J1503+2111	1.9	—	85	J1843+2024	80.5	—
6	J0323+3944	30.2	—	46	J1512−5431	12.7	—	86	J1845−1351	24.9	—
7	J0343−3000	9.8	19.9	47	J1519−6106	54.5	—	87	J1846−4249	29.8	—
8	J0421−0345	73.6	—	48	J1527−3931	31.7	—	88	J1846−7403	3.6	—
9	J0528+2200	11.1	38.7	49	J1528−5547	21.2	—	89	J1848+0604	37.7	—
10	J0546+2441	45.8	—	50	J1615−2940	33	—	90	J1848+1516	6.3	—
11	J0600−5756	20.5	—	51	J1617−4216	29.6	—	91	J1848−1952	27.8	—
12	J0633−2015	33.6	—	52	J1625−4048	13.1	—	92	J1853+0853	27.7	—
13	J0648−27	21.7	—	53	J1629−3636	65.7	—	93	J1857−1027	9.1	—
14	J0737−3039B	24.3	—	54	J1634−4229	22.7	—	94	J1901+0511	29.8	—
15	J0738+6904	20	—	55	J1701−3726	19.1	—	95	J1910+0358	4.3	—
16	J0746−4529	32.3	—	56	J1707−4417	9.9	—	96	J1910+0714	48.4	—
17	J0804−3647	53.2	—	57	J1715−4034	15.1	—	97	J1912+2104	22.4	—
18	J0818−3232	51	—	58	J1732−3729	26.7	—	98	J1915+0752	53.1	—
19	J0847−4316	37.5	—	59	J1736−2457	20.2	—	99	J1917+0834	28	—
20	J0928+06	39.8	—	60	J1741−0840	19.8	58.9	100	J1919+1745	26.1	—
21	J0932−5327	28.2	—	61	J1741−2019	16.2	—	101	J1921−05	20.1	—
22	J0944+4106	21.8	—	62	J1741−21	11.1	—	102	J1945+1211	6.6	—
23	J1001−5939	24.1	—	63	J1743−3150	31.2	—	103	J1951+1123	69	—
24	J1012−2337	24.5	—	64	J1746+2245	20.2	—	104	J2004+3137	53.1	—
25	J1032−5206	30.1	—	65	J1749−2146	13.6	—	105	J2005−0020	32.6	40.8
26	J1049−5833	37.5	—	66	J1750−2043	6.5	—	106	J2015+2524	30	—
27	J1055−6905	26.5	—	67	J1754+5201	15.3	—	107	J2033+0042	13.9	—
28	J1059+6459	35.4	—	68	J1759−1029	6.1	—	108	J2037+1942	32.9	—
29	J1106−6438	58.7	—	69	J1802−3346	26.6	—	109	J2053+4718	32.2	—
30	J1119−7936	40.9	—	70	J1803−1857	58.6	—	110	J2111+2106	28.5	—
31	J1148−5725	36.2	—	71	J1808−2701	25.5	—	111	J2112+4058	23.4	—
32	J1210−6550	35.2	—	72	J1819−17	12.5	—	112	J2131−31	23.5	—
33	J1226−3223	33.8	—	73	J1824−0127	29.2	—	113	J2144−3933	62.9	—
34	J1236−0159	17.4	—	74	J1825−31	12	—	114	J2210+57	11.9	—
35	J1237−6725	55.9	—	75	J1826−1131	23.7	—	115	J2238+6021	42.4	—
36	J1245−6238	26.1	—	76	J1829+25	40	—	116	J2251−3711	66.9	—
37	J1303−6305	27.8	—	77	J1830−1135	17.3	—	117	J2321+6024	12.5	—
38	J1312−6400	43.3	—	78	J1831−1223	17.5	32.6	118	J2323+1241	28.2	—
39	J1314−6101	25.6	—	79	J1831−1329	23.5	—	119	J2324−6054	34.3	62
40	J1355−5747	34	—	80	J1835−0600	38	—				

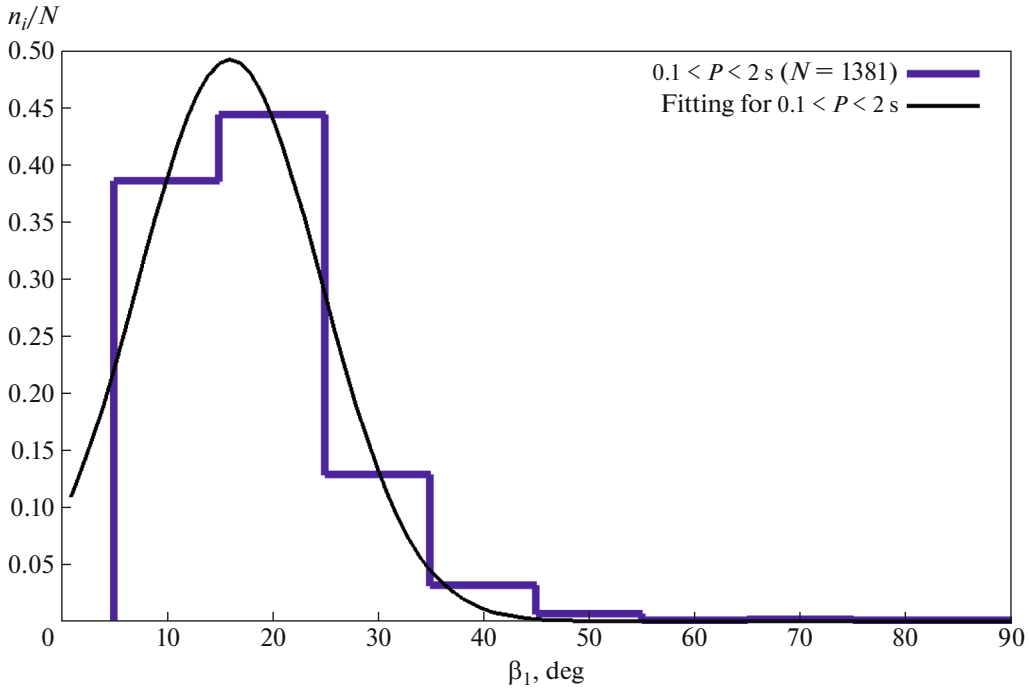

Fig. 6. Angle β_1 distribution for the sample of pulsars with $0.1 < P < 2$ s normalized to the number N of pulsars in the sample.

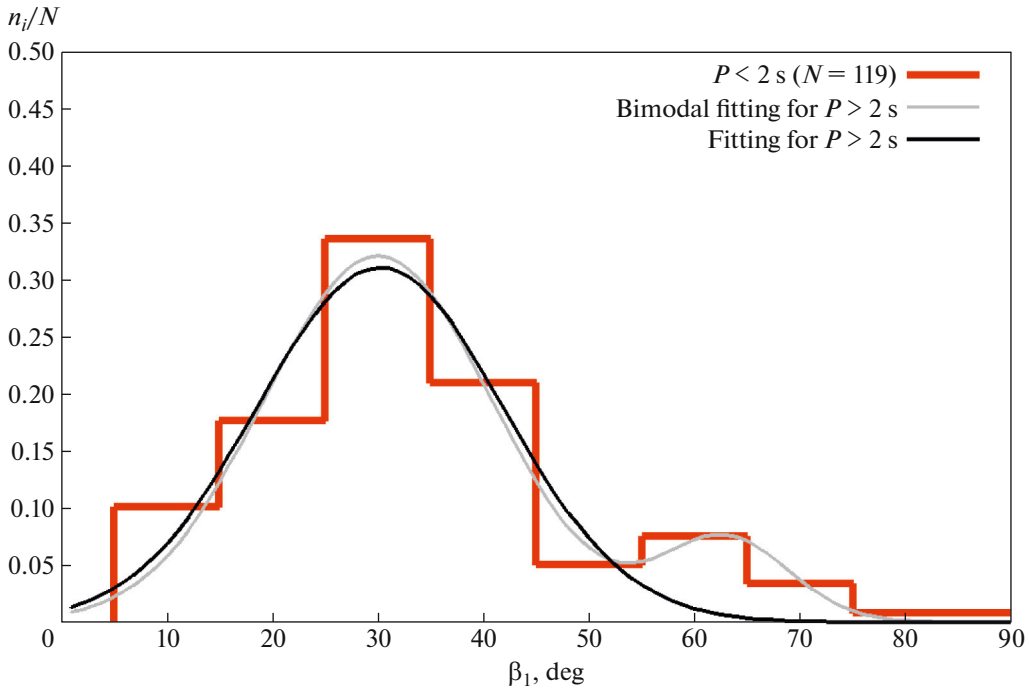

Fig. 7. Angle β_1 distribution for the sample of pulsars with $P > 2$ s normalized to the number N of pulsars in the sample.

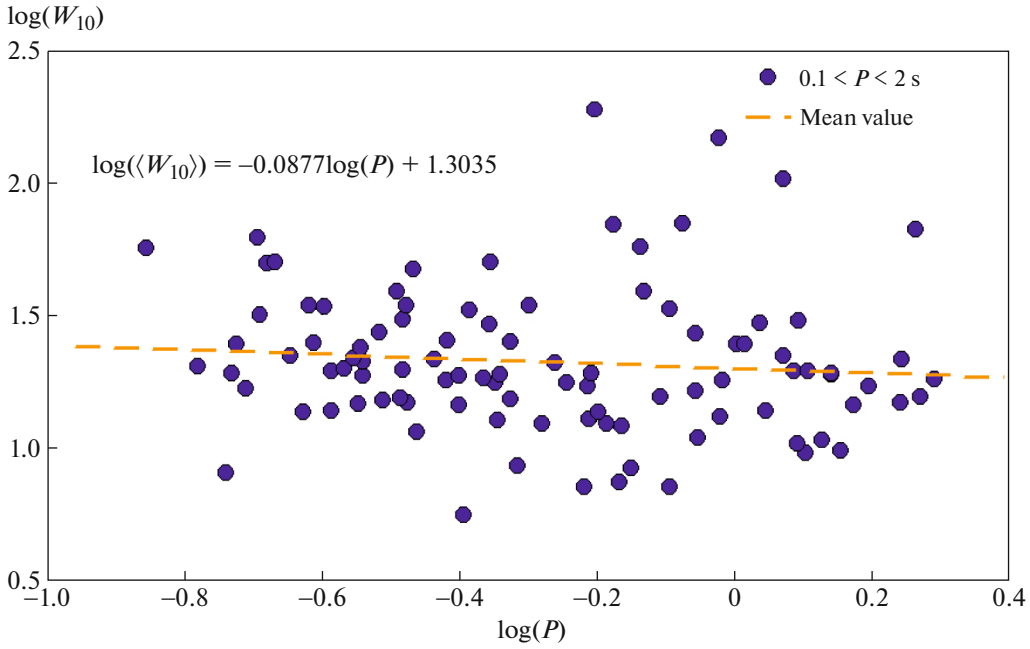

Fig. 8. $\langle W_{10}\rangle$ as a function of period P for the sample with $0.1 < P < 2$ s.

for the sample with $0.1 < P < 2$ s and

$$\frac{n}{N(\beta_1)} = (0.311 \pm 0.036) \times \exp\left\{-\frac{(\beta_1 - (30.2 \pm 1.4))^2}{2(11.7 \pm 3.1)^2}\right\} \quad (20)$$

for pulsars with $P > 2$ s.

For the sample with $P > 2$ s, the distribution of angles β_1 shows a trend for bimodality. The statistical significance of the presence of bimodality was also estimated using the Kolmogorov–Smirnov test. The histogram was compared with two hypotheses: (1) the distribution can be fitted by a single Gaussian (monomodality); (2) the distribution was fitted by two Gaussians (bimodality). The comparison of the histogram with the hypothesis of monomodality yields the Kolmogorov quantile $\lambda = 0.49$, i.e., distributions do not differ significantly with probability $p = 0.97$. Comparing the histogram with the bimodal hypothesis, we obtained $\lambda = 0.33$, which means very good agreement with the model. The visually observed bimodality in the β_1 distribution for $P > 2$ s should be verified again with increased number of pulsars in this interval of periods. It should be emphasized that the currently observed angle β_1 values in the two maxima ($30.0° \pm 1.2°$ and $62.9° \pm 3.5°$) do not overlap with a very high probability (the corresponding variances σ are $10.8° \pm 0.4°$and $6.0° \pm 0.3°$). In addition, the quantile for the bimodal representation is significantly smaller than for the monomodal representation. This means that the bimodal distribution fits the obtained β_1 values much better. For a monomodal distribution with $P > 2$ s, the Gaussian is described by Eq. (20), and for the bimodal hypothesis we can use the approximation:

$$\frac{n(\beta_1)}{N} = A_1 \exp\left(-\frac{1}{2}\left(\frac{\beta_1 - m_1}{\sigma_1}\right)^2\right) + A_2 \exp\left(-\frac{1}{2}\left(\frac{\beta_1 - m_2}{\sigma_2}\right)^2\right),$$
$$A_1 = 0.321 \pm 0.032, \quad m_1 = 30.0 \pm 1.2, \quad \sigma_1 = 10.8 \pm 0.4,$$
$$A_2 = 0.073 \pm 0.003, \quad m_2 = 62.9 \pm 3.5, \quad \sigma_1 = 6.0 \pm 0.3. \quad (21)$$

Figures 8 and 9 show the $\langle W_{10}\rangle(P)$ dependences obtained for both samples of pulsars ($0.1 < P < 2$ s and $P > 2$ s). For the sample with $0.1 < P < 2$ s

$$\log(\langle W_{10}\,[°]\rangle(P)) = -0.088\log(P\,[\text{s}]) + 1.303, \quad (22)$$

which corresponds to

$$\langle W_{10}\rangle = 20.1°P^{-0.09}. \quad (23)$$

For the sample with $P > 2$ s,

$$\log(\langle W_{10}\,[°]\rangle(P)) = -0.998\log(P\,[\text{s}]) + 1.559, \quad (24)$$

hence

$$\langle W_{10}\rangle = 36.2°/P. \quad (25)$$

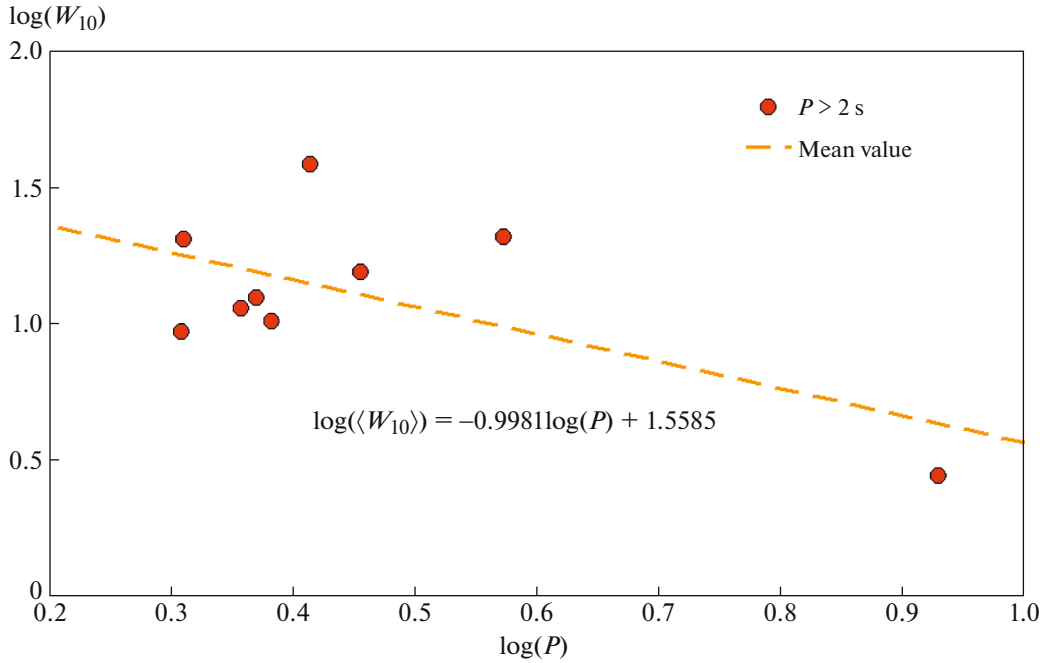

Fig. 9. $\langle W_{10} \rangle$ as a function of period P for the sample with $P > 2$ s.

Since the number of pulsars in the Johnston and Kerr database [14] is several times less than the volume of the ATNF database, the cross-comparison of the catalogs led to a significant reduction in the size of the samples. Further selection of the polarization curves in accordance with the criteria mentioned above reduced the sample size even further. The final analysis included 93 pulsars for the sample with $0.1 < P < 2$ s and 9 pulsars for the sample with $P > 2$ s. The solution of the 4th degree equation gives real roots not for any values B, C, and D, obtained from observations, so the final analysis included 70 pulsars with $0.1 < P < 2$ s and 6 pulsars for the sample with $P > 2$ s. The β angle values calculated by this method (obtained from the solution of Eq. (10)), are denoted as β_2. The histograms of the angle β_2 distributions constructed for the two samples are shown in Fig. 10. The statistical difference between the two distributions was again compared using the Kolmogorov–Smirnov test. The value of the Kolmogorov quantile $\lambda = 0.41$ calculated using formula (18) shows that the β_2 samples for pulsars with $0.1 < P < 2$ s and $P > 2$ s are statistically indistinguishable with a probability $p = 0.996$. This is possibly due to the very small size of the sample with $P > 2$ s.

For the sample with $0.1 < P < 2$ s, the distribution of angles β_2 shows visual signs of bimodality (see Fig. 11). Statistical analysis of the reliability of the presence of bimodality was carried out according to the method described in the previous section. For the case of comparing the histogram with the monomodality hypothesis, the Kolmogorov quantile $\lambda = 0.34$, i.e., the distributions do not differ significantly. Thus, the visually observed bimodality in the β_2 distribution for $0.1 < P < 2$ s is not confirmed in terms of statistical significance. For the monomodal distribution of this sample, $\langle \beta_2 \rangle = 35.6^\circ \pm 4.3^\circ$ ($\sigma = 28.8^\circ \pm 4.1^\circ$).

The fitting of the β_2 distribution with the Gaussian function for the sample with $P > 2$ s gives the mean value $\langle \beta_2 \rangle = 47.6^\circ \pm 5.9^\circ$ ($\sigma = 17.8^\circ \pm 8.0^\circ$), which is shown in Fig. 12. Figures 13 and 14 show the β_1 and β_2 distributions for the two groups of samples. The statistical analysis using the Kolmogorov–Smirnov test showed that for pulsar samples with $0.1 < P < 2$ s, the β_1 and β_2 distributions differ significantly ($\lambda = 2.45$, $p = 0.99999$), while for the β_1 and β_2 distributions of objects with $P > 2$ s, the statistical difference is small ($\lambda = 0.80$, $p = 0.4559$), which may also be due to the small size of the sample with $P > 2$ s for β_2.

Figure 15 depicts the β_1–β_2 diagrams for both samples. The bisector shown by the red line indicates the region on the graph where both methods should give the same result. As can be seen from the graphs, all β_2 values are greater than the corresponding β_1 values (with the exception of four pulsars, for which they can be considered equal within the error limits). The β_1 distribution is noticeably narrower than β_2 (almost three times in the σ value for pulsars with $0.1 < P < 2$ s).

The β_1 values obtained on the basis of formula (6) should be considered as the lower limits of the angle between the rotation axis and the vector of the magnetic moment of the pulsar.

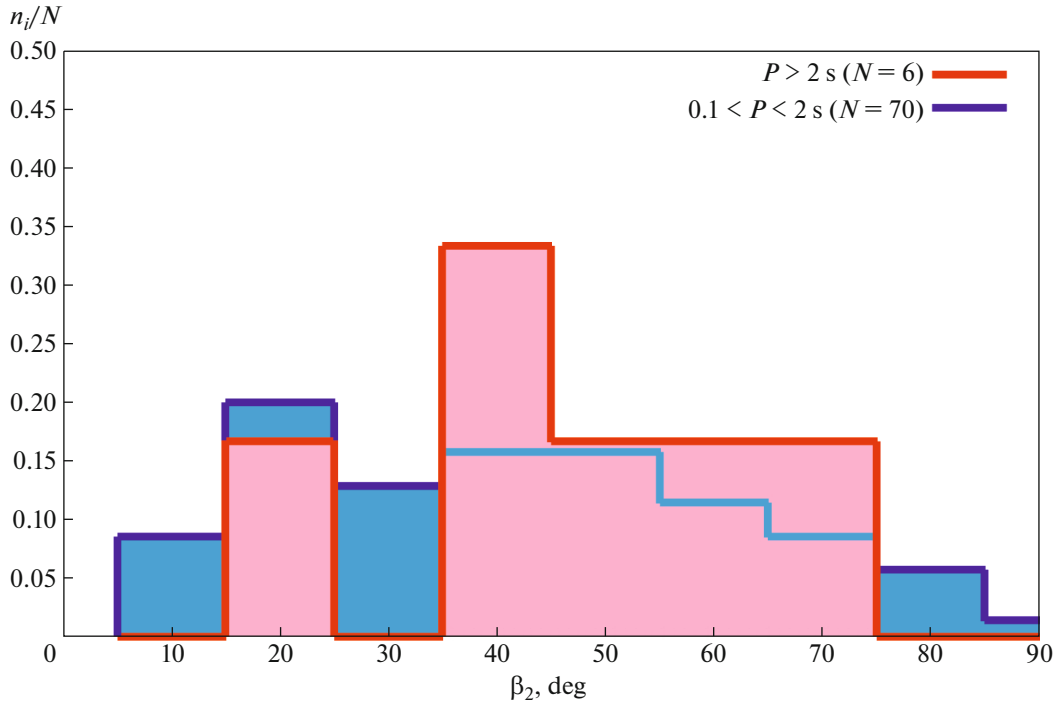

Fig. 10. Angle β_2 distribution histograms for the samples of pulsars with $0.1 < P < 2$ s and $P > 2$ s normalized to the number N of pulsars in the samples.

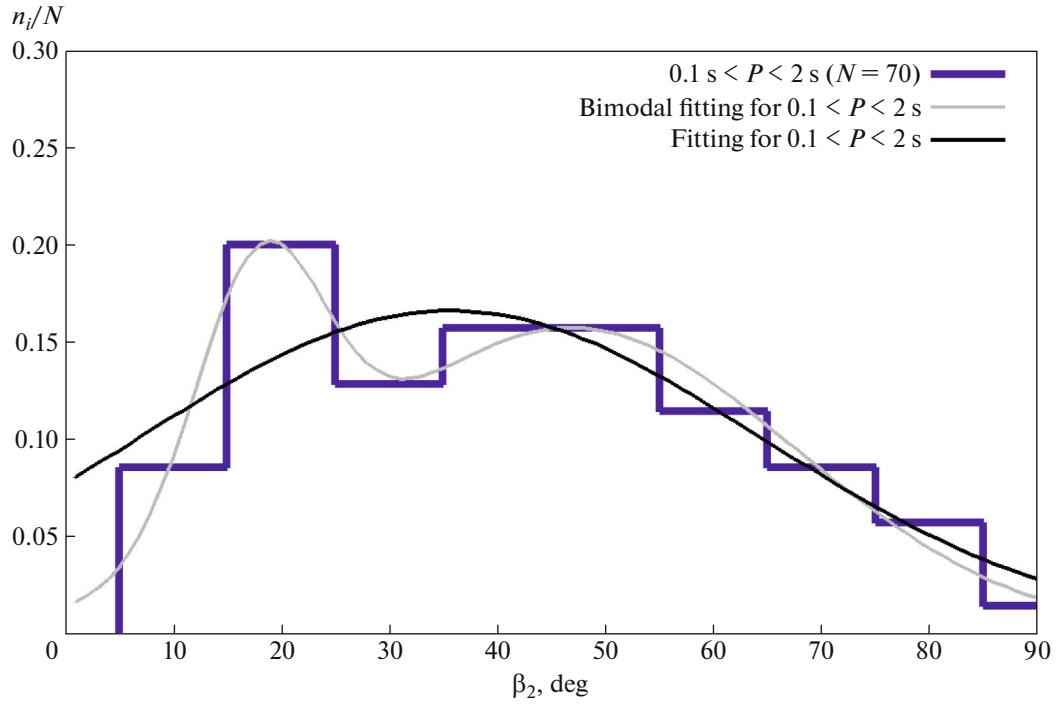

Fig. 11. Angle β_2 distribution for the sample of pulsars with $0.1 < P < 2$ s normalized to the number N of pulsars in the sample.

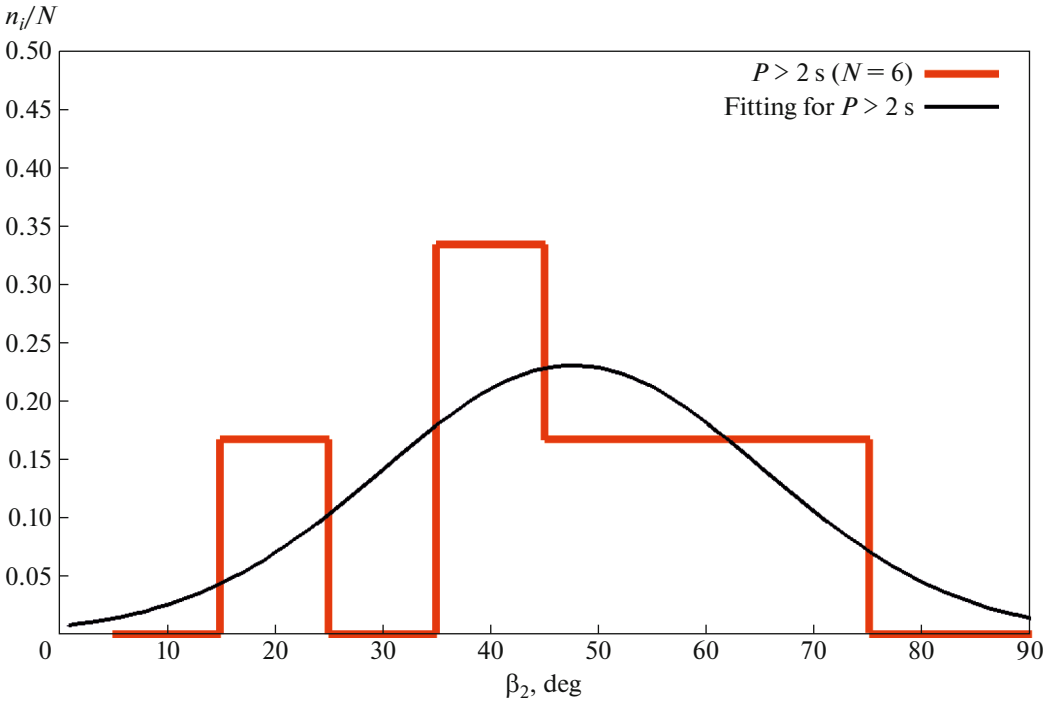

Fig. 12. Angle β_2 distribution for the sample of pulsars with $P > 2$ s normalized to the number N of pulsars in the sample.

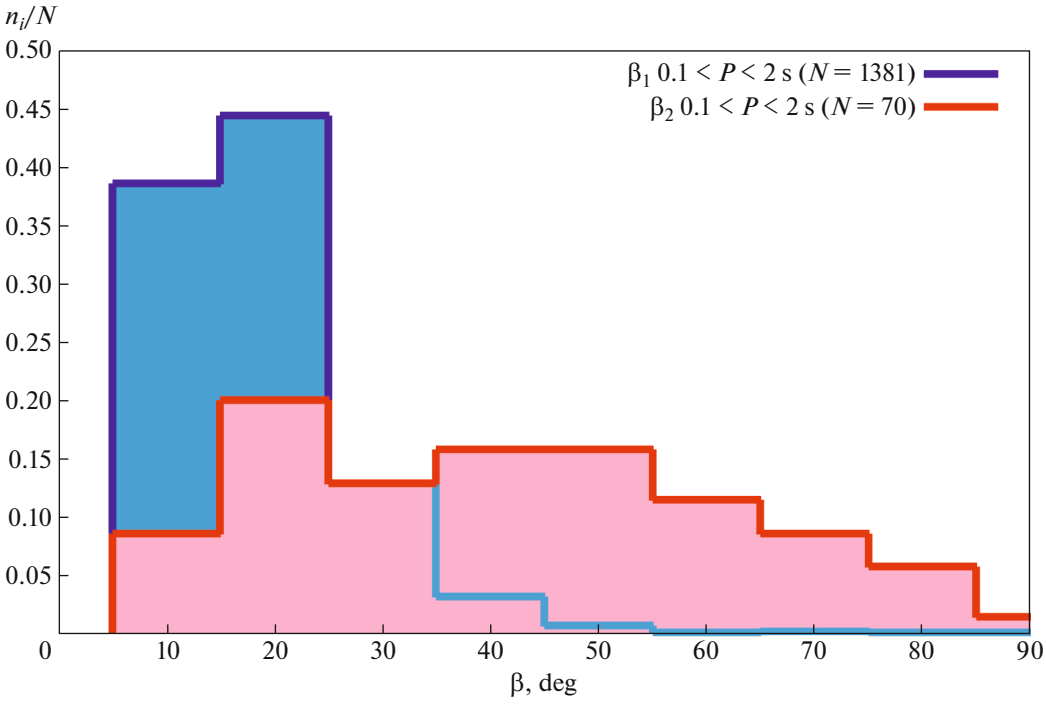

Fig. 13. Distribution histograms of angles β_1 and β_2 for the samples of pulsars with $0.1 < P < 2$ s normalized to the number N of pulsars in the sample.

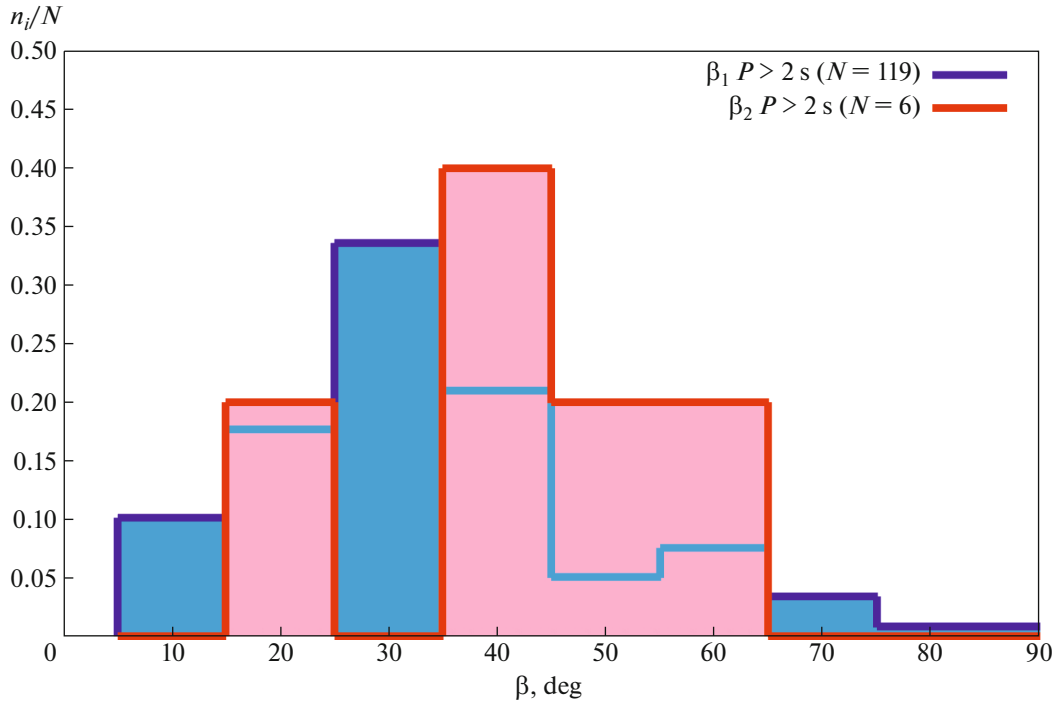

Fig. 14. Distribution histograms of angles β_1 and β_2 for the samples of pulsars with $P > 2$ s normalized to the number N of pulsars in the sample.

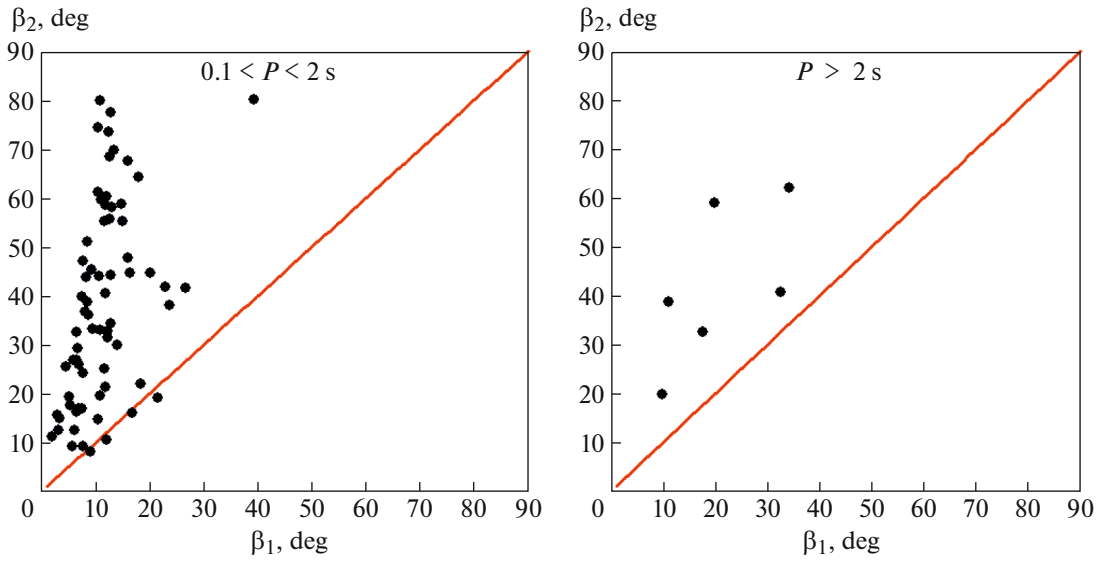

Fig. 15. Angle β_1 and β_2 values for the samples of pulsars with $0.1 < P < 2$ s and $P > 2$ s.

4. DISCUSSION AND CONCLUSIONS

The main goal of our study was to test the possibility of explaining the different behavior of two groups of pulsars with periods $P > 2$ s and $0.1 < P < 2$ s in the (dP/dt)–(P) diagram by the difference in the inclination angle of their magnetic moment to the rotation axis. This possibility was proposed in [1]. Our analysis showed that no such difference was observed. The average values of the lower estimates of angle $\langle\beta_1\rangle = 30.2°$ for pulsars with $P > 2$ s and 16.0° for objects with shorter periods overlap taking into account their variances ($\sigma = 11.7°$ and 8.7°, respectively). The same can be said about more accurate estimates of angle β $\langle\beta_2\rangle = 47.6°$ and 35.6°, $\sigma = 9.5°$ and 10.2°. In both methods, the average value of angle β for pulsars with longer periods turns out to be larger,

which, in accordance with Eq. (2), should rather indicate an increase in their magnetic dipole radiation. Therefore, it is necessary to look for other causes of the observed difference.

We compared the role of two deceleration mechanisms associated with the pulsar wind and magnetic radiation. The corresponding loss of angular momentum is described by Eqs. (1) and (2) above. The ratio of the efficiencies of each of the mechanisms is determined by the following expression:

$$\xi = \frac{(6L_p c^3)^{1/2} P^2}{4\pi^2 B R_*^3 \sin^2\beta}. \quad (26)$$

Assuming that all the characteristic parameters of the pulsars (L, B, R_*, and β) in the two groups are the same, we arrive at the relation

$$\frac{\xi_2}{\xi_1} = \frac{P_2^2}{P_1^2}. \quad (27)$$

The mean periods for the two groups are approximately 2.5 and 0.5 s. This means that the losses due to the pulsar wind in long-period pulsars should be 25 times higher than the magnetic dipole losses. As shown in [1], this is indeed observed.

(1) Our analysis shows that the distribution of β angles calculated by the observed pulse profile width (β_1) confirms the statistically significant difference in the distributions for the pulsar samples with $0.1 < P < 2$ s (sample size $N = 1381$ pulsars) and $P > 2$ s ($N = 119$). At the same time, for the sample with $0.1 < P < 2$ s, the average value $\langle\beta_1\rangle = 16.0° \pm 0.2°$ ($\sigma = 8.7° \pm 0.3°$), and for $P > 2$ s, $\langle\beta_1\rangle = 30.2° \pm 1.4°$ ($\sigma = 11.7° \pm 3.1°$).

The visually observed bimodality in the β_1 distribution for the sample with $P > 2$ s has a low statistical significance according to the Kolmogorov–Smirnov test. However, the Kolmogorov quantile for the bimodal representation is much smaller than for the monomodal one. This means that the bimodal distribution fits the obtained β_1 values better.

(2) The analysis using the maximum derivative of the position angle of polarization yields distributions of angles β_2 that differ noticeably from the corresponding distributions for β_1: $\langle\beta_2\rangle = 35.6° \pm 4.3°$ ($\sigma = 28.8° \pm 4.1°$) for the pulsar sample with $0.1 < P < 2$ s ($N = 70$) and $\langle\beta_2\rangle = 47.6° \pm 5.9°$ ($\sigma = 17.8° \pm 8.0°$) for the sample with $P > 2$ s ($N = 6$). The β_2 distributions in the two samples are not statistically different according to the Kolmogorov–Smirnov test, which may be due to the small sample size for $P > 2$ s. The emerging bimodality in the β_2 distribution for the sample with $0.1 < P < 2$ s turns out to be statistically insignificant according to the Kolmogorov–Smirnov test.

(3) The β_1 and β_2 distributions for the samples with $0.1 < P < 2$ s differ significantly, while the β_1 and β_2 distributions for the samples with $P > 2$ s are not statistically distinguishable, which can also be due to the small size of the sample with $P > 2$ s for β_2.

(4) All β_2 values are greater than or equal to the corresponding β_1 values (within error), which confirms that the β_1 values should be considered as the lower limits of angle β between the axis of rotation and the magnetic moment vector of the pulsar.

(5) The different behavior of radio pulsars with periods $P > 2$ s and $0.1 < P < 2$ s found earlier in the (dP/dt)–(P) diagram is explained by the different period dependence of the losses for the pulsar wind and magnetic dipole braking and by much faster removal of angular momentum by relativistic particles in long-period pulsars.

To confirm the results obtained in this study, in particular, more definite judgments about the emerging bimodalities in the distributions of angle β, it is necessary to expand the sample of pulsars with periods $P > 2$ s.

CONFLICT OF INTEREST

The authors declare that they have no conflicts of interest.

REFERENCES

1. I. F. Malov and A. P. Marozava, Astron. Rep. **66**, 25 (2022).
2. A. K. Harding, L. Contopoulos, and D. Kazanas, Astrophys. J. Lett. **525**, L125 (1999).
3. J. P. Ostriker and J. E. Gunn, Astrophys. J. **157**, 1395 (1969).
4. A. D. Kuz'min and I. M. Dagkesamanskaya, Sov. Astron. Lett. **9**, 80 (1983).
5. I. F. Malov, Astrofizika **24**, 507 (1986).
6. A. G. Lyne and R. N. Manchester, Mon. Not. R. Astron. Soc. **234**, 477 (1988).
7. J. M. Rankin, Astrophys. J. **352**, 247 (1990).
8. I. F. Malov and E. B. Nikitina, Astron. Rep. **55**, 19 (2011).
9. V. S. Beskin, A. V. Gurevich, and Ya. N. Istomin, Sov. Phys. JETP **58**, 235 (1983).
10. A. Philippov, A. Tchekhovskoy, and J. G. Li, Mon. Not. R. Astron. Soc. **441**, 1879 (2014).
11. I. F. Malov, *Radiopulsars* (Nauka, Moscow, 2004) [in Russian].
12. R. N. Manchester, G. B. Hobbs, A. Teoh, and M. Hobbs, Astron. J. **129**, 1993 (2005). https://www.atnf.csiro.au/research/pulsar/psrcat/.
13. R. Manchester and J. Taylor, *Pulsars* (Freeman, San Francisco, 1977).
14. S. Johnston and M. Kerr, Mon. Not. R. Astron. Soc. **474**, 4629 (2018).

Translated by M. Chubarova